Advances in the Molecular Design of Ionenes for a Diverse Range of Applications

Journal:	*Molecular Systems Design & Engineering*
Manuscript ID	ME-REV-02-2021-000007.R1
Article Type:	Review Article
Date Submitted by the Author:	11-Mar-2021
Complete List of Authors:	Lee, Jae Sang; Arizona State University, Chemical Engineering Hocken, Alexis; Arizona State University, Chemical Engineering Green, Matthew; Arizona State University, Chemical Engineering

This review article meets the needs of “Design, System, Application” by identifying the molecular design criteria that make ionenes accessible and functional for a wide range of applications. The article probes the influence of molecular architecture and chemical composition on microphase separation and morphology and the subsequent impact on ionene performance for energy storage devices. Furthermore, the article discusses how variations in the chemical structure impact the biological toxicity and the various strategies that ionenes can be implemented for biomedical applications. Still yet, recent literature using ionenes for gas separations membranes and how the charge density, backbone chemistry, counterions, and chemical composition control the perm-selectivity and gas transport through membranes made of ionenes. Finally, several interesting studies that make use of ion-conducting materials for solar energy harvesting and fuel cell applications are discussed. In each case, we carefully identified the important application-specific design parameters that must be optimized and connected the ionene performance to molecular-level chemical structure information. We envision that this article can be used to direct future efforts that design ionenes for important societally relevant applications.

Advances in the Molecular Design of Ionenes for a Diverse Range of Applications

Jae Sang Lee, Alexis Hocken, Matthew D. Green

Chemical Engineering, School for Engineering of Matter, Transport, and Energy, Arizona State University, Tempe, AZ 85287, USA

***Corresponding Author**
Matthew D. Green

E-mail: mdgreen8@asu.edu

Abstract

Ionenes are polymers that have charges in their backbone rather than on pendant sites. They can be divided into two overarching categories whether the charge is cationic or anionic, and into two subcategories whether they are segmented or non-segmented polymers. Generally, segmented ionenes exhibit thermoplastic elastomer properties due to their low charge density and phase separation compared to non-segmented ionenes. Non-segmented ionenes have been widely used for the various applications ranging from membrane-based separations to biomedical materials; whereas, segmented ionenes have been mostly studied on a fundamental level. This review focuses on trends in the use of non-segmented ionenes in the above applications and more. Furthermore, it describes the properties of segmented ionenes, with attention to the relationships between the structure and function of the segmented ionenes. Together, this review offers insight into the design of ionenes for use in a diverse set of applications.

Keywords: Ionene, Segmented ionene, Non-segmented ionene, Ionene elastomer, Ionene hydrogel

Table of Contents

1. General information about ionenes

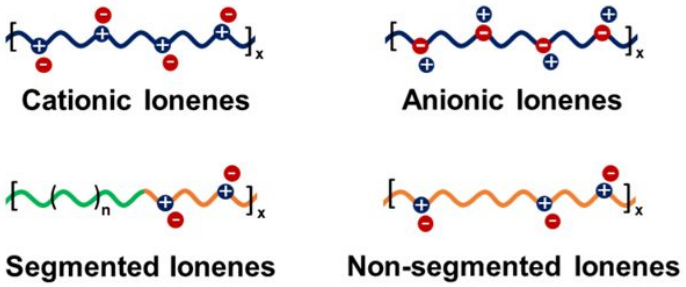

Figure 1. Schematic illustration of cationic and anionic ionenes, and segmented and non-segmented ionenes. Green and orange lines refer to soft and hard segments, respectively.

Ionenes are ion-containing polymers that have charges in the polymer backbone while traditional ionomers and polyelectrolytes have charges pendant to the polymer backbone. Ionenes have received a great deal of attention due to the ability to control the charge density with careful monomer selection and the precise, well-defined spacing of charges in the repeating units. In contrast, ionomers are highly dependent on polymer composition, which presents unequal distributions of ionic groups within a polymer chain, making it challenging to accurately model their behavior.[1] The random distribution of ionic groups in the polymer often complicates the analysis of ionic aggregation effects.[2] Both ionenes and ionomers can be a subset of poly(ionic liquids) (polyILs) that are commonly known as IL-derived polyelectrolytes, but ionenes are typically the product of two neutral monomers that do not show IL formations at any point during the synthesis.[3] In many cases, ionenes are referred to as poly(ILs) or polymeric ILs, which in most cases is incorrect and potentially misleading. Ionenes are also referred to as polyelectrolytes, main-chain polycations, and polyionenes in the scientific literature.[3] Gibbs et al. first synthesized ammonium ionenes via step-growth polymerization of dimethylamino-n-alkyl halides in 1933[4] and Rembaum et al. adopted the name “ionenes” for polymers that contain ionic groups derived from amine-containing

monomers in 1968.[5] Most ionenes in the literature are prepared by step-growth polymerization via the Menshutkin reaction of aliphatic or aromatic ditertiary amines with dihalides.

Most of the ionenes that have been reported are cationic, because synthesizing anionic ionenes has proven to be more challenging.[3] Cationic ionenes containing ammonium, pyridinium, phosphonium, imidazolium, and DABCO-based ions have been synthesized. Polyamide, polyimide, polyester, and polyurethane ionenes can also be synthesized using functional monomers in conventional condensation polymers.[3] Recent reports have shown the successful development of poly(arylsulfonimide) ionenes[6] and poly(perfluoroalkylsulfonyl)imide (PFSI) ionenes[7] from anionic ionenes. They show promise due to their improved thermal stability and unique capabilities, such as having a cationic counterion for Li^+ ion batteries, which are unavailable to cationic ionenes.[3]

Ionenes can be divided into two categories: segmented and non-segmented ionenes, and these can be further classified as either cationic or anionic (as discussed above). Segmented polymers have alternating hard and soft segments along the backbone, created by the polymerization of oligomeric spacers. This configuration produces polymers with excellent mechanical, thermal, and morphological properties.[8] Segmented ionenes are structurally similar, wherein the oligomeric hard segments typically contain the charged domains, which creates interesting design features because of the mechanical and morphological characteristics. Some of the soft segments used to make segmented ionenes include poly(tetramethylene oxide) (PTMO), poly(ethylene glycol) (PEG), and poly(propylene glycol) (PPG) and some of the hard segments used to synthesize segmented ionenes include 1,12-dibromododecane, 4,4'-bipyridine, 1,2-bis(4-pyridium)ethylene, N,N,N',N'-tetramethyl-1,6-hexanediamine, 1,4-diazabicyclo[2,2,2]octane (DABCO), and 1,4-dibromo-*p*-xylene. The soft segments have glass transition temperatures (T_g) below ambient temperature (or below the application temperature)

which provides flexibility and ductility.[9] Kohjita et al. first reported segmented ammonium cationic ionenes with a PTMO soft segment in 1981.[10] Segmented ionenes typically undergo microphase separation, and, due to the low volume fraction of hard segments relative to soft segments, a continuous soft segment matrix with randomly dispersed and isolated hard segments are formed.[9] This microphase separation is attributed to a combination of Coulombic interactions and segment-segment incompatibility, the latter drives microphase separation in block polymers and segmented polymers (e.g., segmented urethanes).[11] Additionally, crystallization contributes to this separation, which is a function of soft segment molecular weight, volume fraction (relative to the hard segment), and the propensity of the hard and soft segment to crystallize.[12] The mechanical properties of segmented ionenes were found to be dependent on both the nature and the amount of the hard segment.[13] Hard segment contents over 25 wt% incurs connectivity between the hard domains, which can become percolated throughout the matrix.[9] Segmented ionenes have been compared with polyurethanes (PU) because segmented ionenes show high tensile strength and high elongation which mechanically resemble segmented PU.[14] However, segmented PUs are prepared with toxic isocyanates using a two-step process. In contrast, segmented ionenes are potentially more environmentally friendly, use safer precursors, and are synthesized in a single step process. Segmented PUs need more than one hard segment moiety within a hard segment microdomain to have sufficient microphase separation to enhance the physical properties, whereas segmented ionenes can obtain decent phase separation with a single unit of the ionene hard segment.[11]

The most common type of non-segmented ionenes is an aliphatic ammonium ionene, and it is usually synthesized via the Menshutkin reaction. Aliphatic, non-segmented ammonium ionenes use the following nomenclature: x,y-ionenes, where x and y indicate the number of methylene units in the diamine and dihalide monomers, respectively.[15] The varying

charge density can result in different properties of ionenes which can be tuned by varying x and y. For example, non-segmented ionenes are usually brittle materials that show poor mechanical properties due to the high charge density, but the polymer solubility and stability in water-salt media can be tailored with the value of x and y.[16,17] Rembaum and Noguchi revealed that monomers with a low number of methylene spacers (i.e., x,y- equal to 2,1-, 2,2-, 2,3-, or 3,2-) can produce low molecular weight cyclic ionenes.[15] The choice of solvent, reaction temperature, reaction time, and the concentration of the monomer during the polymerization of the non-segmented ionenes all impact the polymerization.[1]

The type of counterions, charge distribution, molecular weight, structural flexibility, and H-bonding capability are critical aspects that may affect the dynamics of the ionic chains that govern ionene properties.[18] The majority of ionenes that have been studied are cationic with varying halide anions (e.g., fluoride (F^-), chloride (Cl^-), bromide (Br^-) and iodide (I^-)[19]). Other counterions, such as hexafluorophosphate (PF_6^-), tetracyanoquinodimethane ($TCNQ^-$), tetrafluoroborate (BF_4^-), trifluoromethanesulfonate ($CF_3SO_3^-$), and bis(trifluoromethanesulfonyl)imide (Tf_2N^-), have been studied as well.[20,21] Meanwhile, there are only a few anionic ionenes with a cationic counterion; for example, lithium (Li^+), that have been reported.[22,23] Generally, smaller anions attract more water molecules, resulting in a tight hydration shell close to the quaternary nitrogen. Whereas, the larger counterions do not create such a tight shell, resulting in ions that are closer to the ionene chain according to molecular dynamics simulations of non-segmented ammonium 3,3-ionenes.[24] Peter et al. studied the influence of counterions on ion-binding with 3,3-, 6,6-, and 6,9-ionenes, which are aliphatic, cationic, ammonium, and non-segmented ionene.[25] The association of the counterions to the ionene backbone, cationic or anionic, strongly depends on the charge density of the ionene and the chemical nature of the counterions. The strongest effect of charge density and counterion

effects is demonstrated in ionene solutions when the counterion is changed from Br^- to F^-. Miha et al. estimated the self-diffusion coefficients of the Br^- and F^- counterions associated with 3,3-, 4,5-, 6,6- and 6,9-ionenes in water.[26,27] The F^- and Br^- counterions preferred longitudinal and transverse fluctuation, respectively, with respect to the polyelectrolyte backbone. This means that F^- counterions prefer to move along the shorter segment of the chain backbone, while Br^- counterions prefer to fluctuate radially to the backbone. The F^- counterions keep their hydration shell intact when approaching the ionene and behave like a charged hard-sphere with a hydrated radius, whereas Br^- counterions give away the hydrated water in order to interact with the ionene. Thus, the water associated with the Br- counterion is loosely bound due to the chaotropic nature of Br^- ions. The T_g of ionenes is dependent on molecular weight and the chemical structure but also the size and shape of the counterions.[28] Small spherical anions such as BF_4^- decreased T_g, while large counterions, tetraphenylborate (BPh_4), or ethyl-orange sulfonate (EO) led to higher T_gs.[29]

The Hofmann elimination reaction is the most common degradation mechanism for ionenes. It depends on the basicity of the counterions; ionenes with less basic counterions degrade at higher temperatures compared to stronger base counterions.[28] Although decomposition reactions of polymeric ammonium salts are more complicated due to many competing mechanisms occurring in the polymer chain,[30] several ionene degradation processes have been known such as the reverse Menshutkin reaction, nucleophilic substitution reaction, and Hofmann elimination reaction that eliminate alkyl substituents from quaternary salts. Charlier et al. revealed that quaternized ammoniums can have a better thermal stability than tertiary amines.[31] Specifically, the amines degraded at 180 ℃, but high charge density aliphatic ionenes are stable to ~250 ℃.[32] Ionenes undergo Hofmann elimination and reverse Menshutkin reactions at elevated temperature via anion attack on the ammonium cation. The effect of other

factors on the ionenes' properties will be further discussed below in the context of different types of ionenes.

Bara and O'Harra reviewed the current state of the art for ionenes in 2019,[3] which established a clear definition of ionenes (among polyelectrolytes) and provided key lessons for designing anionic and cationic ionenes. However, there is still a gap in the establishment of structure-property-function relationships for ionenes at the interface of various applications. Specifically, limited analysis of the properties of segmented ionenes exists, which currently limits their implementation in diverse applications. This review will summarize the use of non-segmented ionenes in several widely reported applications and provide the properties of the non-segmented ionene hydrogels. Furthermore, it will create design rules for structure-property-function relationships for segmented ionene elastomers.

2. Non-segmented ionenes

Here, a review of non-segmented ionenes is provided to study structural differences that introduce properties for membrane separations, biomedical therapeutics, and energy storage. This review will provide context for the discussion of segmented ionenes later.

2.1 Applications

2.1.1. Membrane-based separations

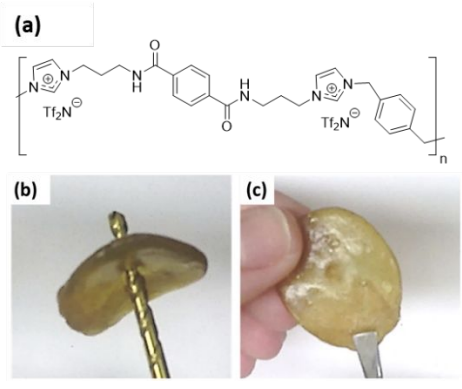

Figure 2. (a) Structure of imidazolium-based polyamide ionenes with both amide and xylyl linkages in *para*- positions and illustration of (b) before and (c) after self-healing characteristic of ionene film.[33] Reproduced from Ref. 33 with permission, copyright 2019 John Wiley and Sons.

Non-segmented ionenes have been implemented as membranes for gas separations, CO_2 capture, and humidity sensing. Kammakakam et al. introduced imidazolium-based polyamide ionenes containing Tf_2N^- counterions and revealed that both amide and xylyl linkages attached at *para*- or *meta*- positions resulted in higher perm-selectivity for CO_2/CH_4 and CO_2/N_2 gas pairs owing to the high CO_2 solubility.[33] However, the permeability of all structural combinations was low relative to controls. When both the amide and xylyl groups were attached in the *para*- position (**Figure 2a**) the membranes showed the highest permeability, possibly due to the lower T_g and looser inter-chain packing. This polymer also showed a self-healing property due to the ionic interactions between imidazolium cations and counteranions as well as hydrogen bonding between amide groups (**Figure 2b and c**). They also described imidazolium-based polyimide ionenes that contained the N,N′-bis(3-imidazol-1-yl-propyl)pyromellitic diimide and *p*-dichloroxylene with Tf_2N^- counterions that were soaked with an IL, $[C_4mim][Tf_2N]$, for gas separation.[34] The ionic polyimides absorbed IL into their structures at ambient temperature, which increased the permeability of CO_2, N_2, and CH_4 by 1800-2700% due to increased gas diffusivity while the gas solubility remained unchanged with the IL present. It is noteworthy that Tf_2N^- counterions have been widely used for gas separation due to their ability to solubilize CO_2.[35]

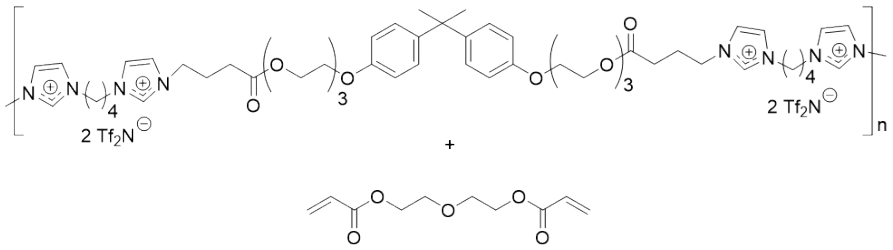

Figure 3. Structure of the imidazolium-based ionenes made from bromine-terminated bisphenol poly(ethylene glycol) (PEG) and 1,4-di(1H-imidazol-1-yl)butane that are then crosslinked within a di(ethylene glycol)diacrylate to form a composite network.[35]

Ionenes have also been incorporated into networks and thermosets. For example, an ionene prepared by reacting 1,4-di(1H-imidazol-1-yl)butane and bromine-terminated bisphenol poly(ethylene glycol) was loaded into a composite blend network by crosslinking di(ethylene glycol)diacrylate (DEGDA) around the ionene (**Figure 3**).[35] The low molecular weight DEGDA matrix provided mechanical stability and CO_2 affinity to the membrane. A 2:1 ratio of ionene:DEGDA showed the highest permeability to all gases including CO_2, O_2, and N_2, and a 3:1 ratio yielded the highest CO_2/N_2 perm-selectivity. However, all of the networks exhibited a low gas permeability, and it was suggested that a longer PEG linker in the ionene and/or the crosslinker could improve the gas permeability.

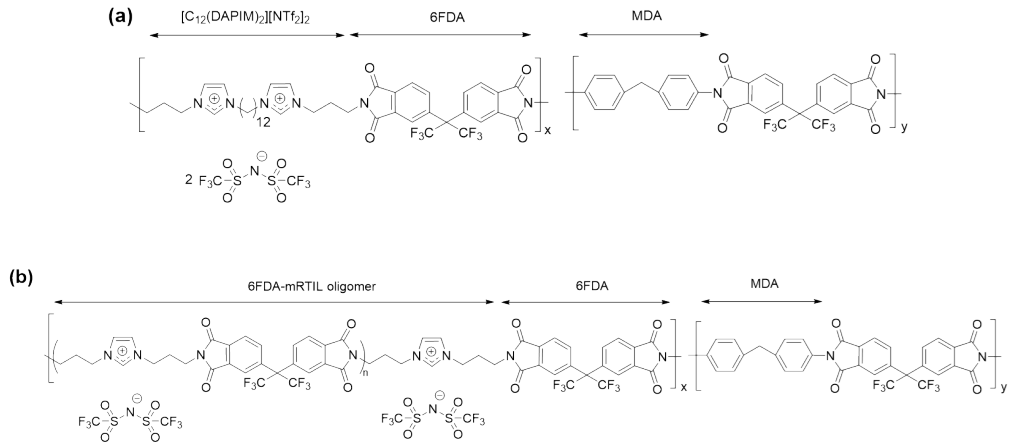

Figure 4. Structures of the imidazolium-based copolyimide ionenes having (a) two and (b) one imidazolium ring synthesized by Li et al.[36,37]

Li et al. reported imidazolium-based copolyimide ionenes made from 2,2-bis(3,4-carboxylyphenyl)hexafluoropropane dianhydride (6FDA), *m*-phenylenediamine (MDA), and 6FDA-1,12-di[3-(3-aminopropyl) imidazolium] dodecane bis[(trifluoromethyl)sulfonyl]imide ($[C_{12}(DAPIM)_2][Tf_2N]_2$) (diRTIL), which produced a random copolyimide with two imidazolium rings in the backbone (**Figure 4a**) and Tf_2N counterions.[36] Whereas, reacting 6FDA, MDA, and 6FDA-[DAPIM][NTf_2] (6FDA-mRTIL) oligomer produced a copolyimide with one imidazolium ring in the backbone (**Figure 4b**).[37] The thermal stability, T_g, d-spacing, and fractional free volume (FFV) decreased upon increasing the concentration of 6FDA-mRTIL oligomer, whereas the polymer density increased gradually. Furthermore, gas permeability, solubility, and diffusivity decreased and perm-selectivity of CO_2/CH_4, H_2/CH_4, and O_2/N_2 gas pairs increased by the incorporation of diRTIL within the 6FDA–MDA backbone. The diRTIL copolymer exhibited a lower perm-selectivity than the mRTIL copolymer, however, both copolyimide ionenes showed a higher ideal CO_2/CH_4 perm-selectivity when compared to 6FDA-MDA. O'Harra et al. incorporated 6FDA into imidazolium-based polyimide ionenes with different structural isomers of xylene and the imidazolium monomer.[38] The -CF_3 groups in 6FDA were able to prevent large chain packing, thus producing a high FFV that enhanced the gas permeability. Interestingly, ionenes made from monomers with para-linkages on both xylene and the imidazolium monomer (**Figure 5**) displayed the highest value of M_n, which the authors attribute to less steric hindrance when compared to ionenes synthesized from monomers with ortho- and meta- linkages. The para-linked polymers also showed the highest d-spacing, which gives insight into the packing efficiency and thus predicts the permeability.

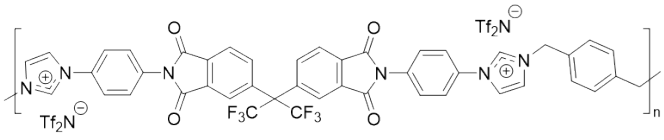

Figure 5. Structure of imidazolium-based polyimide ionenes with both imidazolium moiety and xylyl linkages in *para*- positions synthesized by O'Harra et al.[38]

Phosphonium salts typically exhibit enhanced thermal stability relative to quaternary nitrogen-based salts such as imidazolium, ammonium, and pyridinium due to the phosphonium cation's resistance to the reverse Menshutkin degradation and Hofmann elimination.[39] The Hofmann elimination generates an unsaturated alkane and a tertiary amine when the basic counterion attacks the β-carbon (relative to the ammonium ion). However, the phosphonium cation degrades into a tertiary phosphine oxide and alkane under alkaline conditions.[40] Yang et al. prepared phosphonium-based ionenes for CO_2 capture membranes as well as alkaline fuel cell (AFC) membranes.[41] They formed a polymer network using (4-acetylphenyl)diphenyl phosphonium bromide (M1) and 1,4-diacetylbenzene (M2) with Tf_2N^- counterions (**Figure 6**), which displayed an improved thermal and alkaline stability when compared to linear analogs. Furthermore, the ratio of charged (M1) and uncharged (M2) moieties affected the porosity and surface area of the material, a 1:2 ratio exhibited enhanced CO_2 uptake affinity and the values were comparable to analogous non-network and non-phosphonium materials.

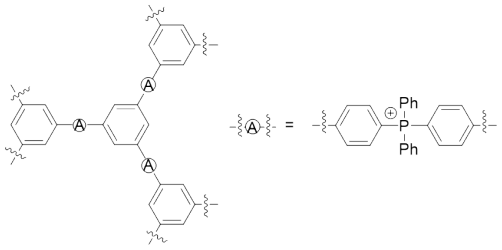

Figure 6. The structure of a phosphonium ionene polymer network synthesized by Yang et al.[41]

Williams et al. introduced the potential of using 12,12-ammonium-based ionenes as membranes with tunable mechanical properties (**Figure 7a**); the introduction of a cinnamate end group allowed for a UV light-mediated crosslinking reaction (final product shown in **Figure 7b)**.[42] Jeon and Gong reported ammonium-based ionenes for humidity sensing membranes by incorporating 3-(trimethoxysilyl)propyl methacrylate into 4,6-ammonium ionenes to introduce methacrylate end groups (**Figure 7c**).[43] Coating the synthesized ammonium ionenes on the surface of a sensor electrode through the photo-initiated radical polymerization exhibited an improved sensor durability and stability of the humidity sensitive membrane at elevated temperature and humidity. Gong developed ammonium-based ionenes containing a photocurable polyester and aromatic benzyl group as shown in **Figure 8.**[44] The 2,2-ionenes functionalized with a hydroxybenzyl end group and Br^- counterions were copolymerized with 4,4'-dihydroxy chalcone and terephthaloyl chloride to form ammonium-based polyester ionenes. The ionenes functionalized with hydroxybenzyl group were hygroscopic, and the chalcone group could successfully be crosslinked by UV irradiation.

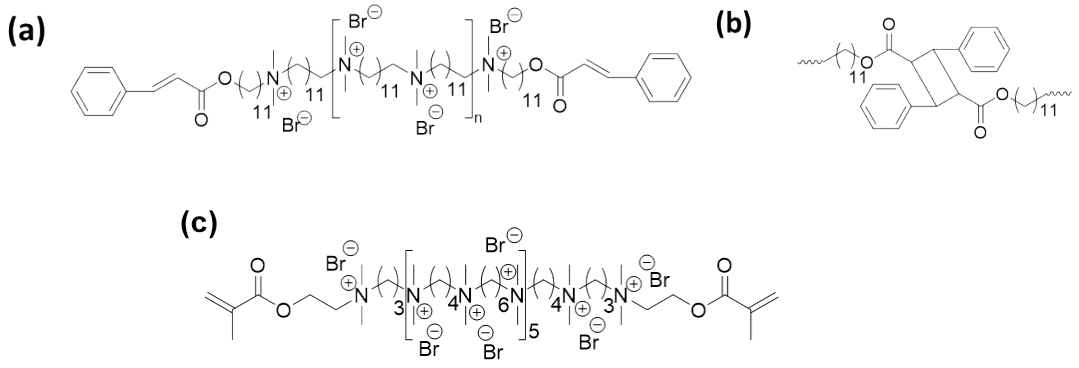

Figure 7. Structures of (a) cinnamate-functionalized 12,12-ammonium ionenes, (b) light-mediated crosslinked ammonium ionene network by Williams et al.,[42] and (c) 4,6-ammonium ionenes with methacrylate end groups synthesized by Jeon and Gong.[43]

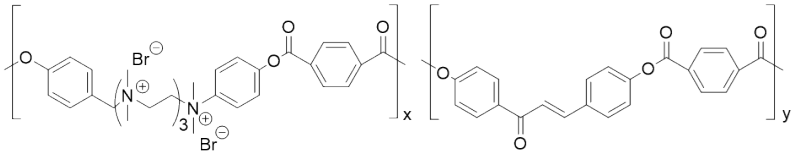

Figure 8. Structure of the photo-curable copolymerized ammonium-based copolyester ionenes synthesized by Gong.[44]

2.1.2. Biomedical materials and devices

Non-segmented ammonium-based ionenes have been reported in various biomedical applications. The polyelectrolyte complex (PEC) of DNA and ionenes or ionomers is promising for the delivery of genetic material (i.e., gene delivery) due to a lack of immunogenicity, the ability to tailor the complex's properties, and electrostatic attraction of the complex with the slightly negatively charged cellular membranes.[45] An important consideration in designing ionenes to form PECs is the biocompatibility or cytotoxicity of the polymer. Ionenes with a lower charge density and longer hydrophobic segment have been shown to destroy the cell regardless of the amount of polymer bound to the cell membrane. The hydrophobicity of the polymer plays a more critical role in cell disruption when compared to the polymer's charge density, as revealed by cytotoxicity studies performed using a series of x,y-ionenes (x=3, 6 or 12; y=3, 4, 6, or 12) and x,X-ionenes (x=3, 6 or 12, X=xylylene), all of which contained Br^- counterions.[46] The higher polymer charge density proved to promote cell binding but does not destroy the cell.

The stability of the PEC in various relevant conditions (e.g., high salt concentrations, presence of multivalent salts, and varying protein concentrations) is dependent on the type of charge contained in the ionene as well as the number of methylene units, the polymer chain length, and the charge density.[47–50] Zelikin et al. reported that although it is not universally true that charge density in linear ionenes is a factor in controlling the stability of PEC, they did show that the stability of the PEC increased when charge density increased and the chain

shortened.[45] Wahlund et al. compared phase separation of PECs containing either DNA or RNA with 2,5-ionenes containing Br^- counterions.[51] The strong binding of Br^- counterions and relatively low molecular weight (average DP is 40) caused the PEC to precipitate.

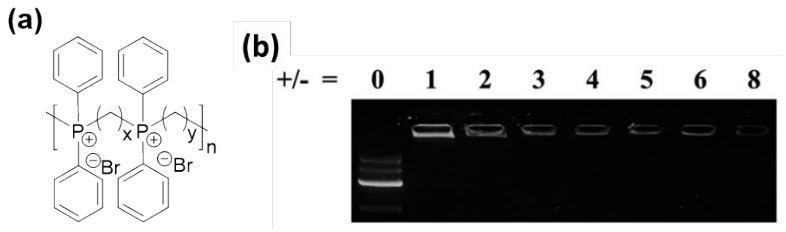

Figure 9. (a) Structure of phosphonium-based ionenes synthesized with bis(diphenyl)phosphines and dibromides and (b) DNA binding efficiency of 6P,6-ionene.[39] Reproduced from Ref. 39 with permission from the Royal Society of Chemistry.

Hemp et al. synthesized phosphonium-based ionenes with Br^- counterions from bis(diphenyl)phosphines and dibromides (**Figure 9a**), which exhibited poor water solubility due to the presence of the phenyl group attached to the phosphonium cation.[39] However, it dissolved in water at 100 ℃ and remained soluble at room temperature, and thus it could be easily applied to DNA binding studies. The 6P,6-ionene (in xP,y-ionene the x and y indicate the length of the methylene space in the ditertiary phosphine and dihaloalkane, respectively) effectively bound plasmid DNA at a phosphonium:phosphate ratio of 1:1 as shown in **Figure 9b**.

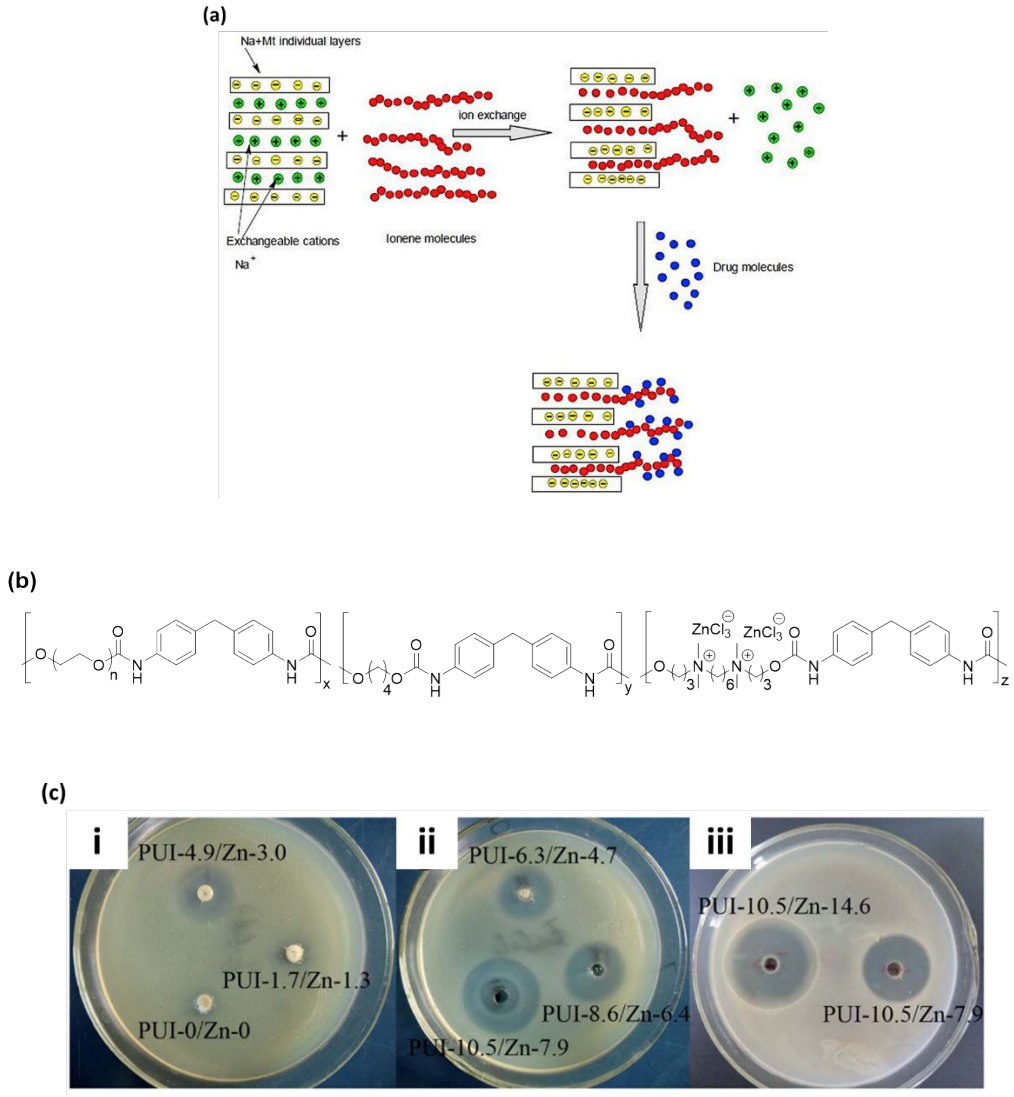

Figure 10. (a) Scheme of a drug release system using ammonium ionenes. Montmorillonite (Mt) works as a drug carrier by forming a nanocomposite with ionenes.[52] Reprinted from Ref. 52, Copyright 2019, with permission from Elsevier. (b) Structure of the polyurethane ionenes with 1,4-butanediol, 4,4'-diphenylmethane diisocyanate and PEG 4K, and (c) images of the inhibition zones against E. coli growth (i, ii = 48 h and iii = 72 h).[55] Reproduced from Ref. 55 with permission from the Royal Society of Chemistry.

Ionenes have also been studied for use in controlled release systems with applications including drug release for biomedical therapies as well as pesticide release for agricultural purposes. For example, the anti-inflammatory drug, diclofenac sodium, was immobilized onto the ammonium-based ionenes as shown in **Figure 10a**.[52] The ionene-drug complex exhibited a slower drug release profile compared to a simple quaternary ammonium salt owing to the

entrapment of the drug molecules in the entangled ionene chains that slowed down the diffusion. Ionenes have also been studied as antimicrobials; the strong electrostatic interaction between the ionene and bacteria as well as the hydrophobic alkyl chains that make up the backbones of many ionenes, specifically those alkyl spacers with eight or more carbon atoms, facilitate the diffusion of cationic ionenes into bacterial cell membranes.[53–55] As an example, Ding et al. prepared segmented polyurethane ionenes (PUIs) with ammonium-based ionene segments containing $ZnCl_3^-$ counterions (which may exist in a dimeric form $Zn_2Cl_6^{2-}$) and used them as antimicrobial application (**Figure 10b**).[55] The $ZnCl_3^-$ ionenes produced an inhibition zone for both gram-positive and gram-negative bacteria, which increased with an increase in $ZnCl_3^-$ content as shown in **Figure 10c**. However, Cakmak et al. used simple ammonium-based ionenes with Cl^- counterions that exhibited a higher inhibition zone for gram-positive bacteria compared to gram-negative bacteria.[56] An increase in ionene concentration ultimately inhibited all bacterial growth. The linker chemistry also affected the antimicrobial properties and as ionenes with amide bonds were more lethal (>99.9%) at a lower concentration than when ester bonds were incorporated.[57] Geng and Finn revealed a new class of antimicrobial ionenes by introducing thiabicyclo[3.3.1]nonane in pyridinium-based ionenes.[58] Furthermore, Strassburg et al. utilized 3,4-ammonium ionenes with Br^- counterions as an antimicrobial functional structure within an interpenetrating hydrogel for the suppression of bacterial growth in wound healing (**Figure 11**).[59] Even a low concentration of ionenes successfully killed all adhered bacterial cells on the hydrogel for a period of up to 4 weeks. Also, hydrogels using acrylamide and chloromethylstyrene-functionalized 2,4-ionenes with Br^- counterions showed promise for cell binding, drug delivery, and antimicrobial applications due to the high charge density and hydrophobicity as well as the improved mechanical properties compared to nonionic copolymers.[60] Ionenes showed outstanding skin compatibility with low *in vivo* toxicity,[61]

suggesting that ionenes could be used as non-alcohol based and non-dehydrating surgical scrubs and hand sanitizers.

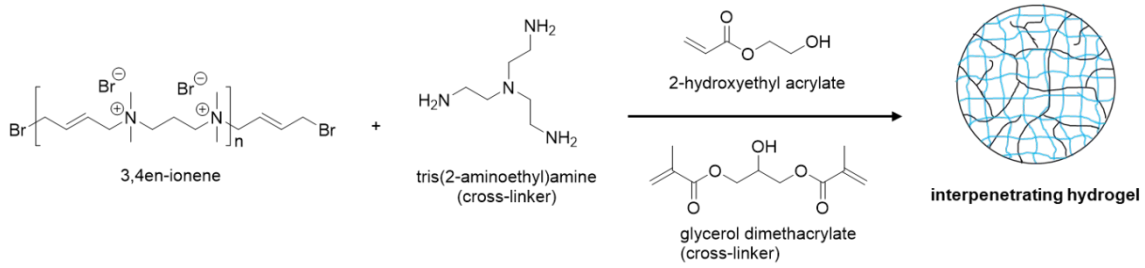

Figure 11. Schematic showing the fabrication of an interpenetrating hydrogel with 3,4en-ionenes.[59] Reprinted with permission from Ref. 59. Copyright 2017 American Chemical Society.

2.1.3. Materials for Solar cells and Batteries

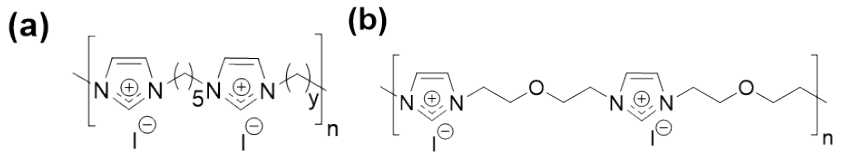

Figure 12. (a) Imidazolium-based ionenes synthesized with 1,1'-(1,5-pentamethylene)bis(imidazole) and diiodobutane (y = 4 or 6) by Suzuki et al.[19] and (b) structure of the alkyloxy imidazolium ionene synthesized by Li et al.[65]

Imidazolium-based ionenes have been used as polymer electrolytes in dye-sensitized solar cells (DSCs) and Li-ion batteries.[62–64] For example, Suzuki et al. achieved a 1.3% photon to electron conversion efficiency in the cells containing ionenes.[19] Since solidifying liquid electrolytes can reduce electrolyte leakage and evaporation, they synthesized imidazolium-based ionenes with I^- counterions (xI,y-ionenes, where x and y indicate the length of the methylene space in the imidazolium and dihaloalkane, respectively). It was regarded as a molten salt type polymer that was suitable for quasi-solidification of IL electrolytes of DSCs by combining 1,1'-(1,5-pentamethylene)bis(imidazole) with 1,4-diiodobutane or 1,6-diiodohexane as shown in **Figure 12a**. Moreover, Li et al. used alkyloxy imidazolium-based

ionenes containing I^- counterions (**Figure 12b**) that mixed two monomers, 1,1'-(2,2'-oxybis(ethane-2,1-diyl))bis(imidazole) and diethylene glycol diiodide, and encapsulated ILs, 1-methyl-3-propylimidazolium iodide (MPII) or 1,2-dimethyl-3-propylimidazolium iodide (DMPII), as a quasi-solid electrolyte for DSCs.[65] The MPII encapsulated ionenes exhibited better light-to-electricity conversion efficiency than DMPII. The addition of MPII provided better conversion efficiency, stability, and conductivity on DSCs.[66] Ionenes satisfy the need for a high ionic conductivity and good mechanical strength in DSCs, and the ability to fabricate them with liquid electrolytes, including ILs, has attracted attention to this promising material class.

The use of ionenes improved the performance of lithium-ion batteries (LIBs) by improving the electronic and ionic conductivity of the cathodes. PFSI ionenes (**Figure 13a**, ammonium-based polyimide ionenes) have been used in several ways to improve the battery performance as its backbone provides a low lithium dissociation energy and high cationic exchange capacity.[67] The anionic aliphatic PFSI ionenes with Li^+ counterions mixed with poly(vinylidene difluoride) (PVDF) exhibited a higher energy density and better reversibility than when only PVDF was used.[7] Shi et al. prepared PFSI ionenes with Li^+ counterions mixed with PEG as shown in **Figure 13b;** the perfluoroether connector, $-CF_2CF_2OCF_2CF_2-$, sustained a high ionic conductivity and lithium-ion transport number.[67] Also, perfluoroether connector gave a better compatibility between flexible ionene and PEG segments that enhanced long-term electrochemical stability.

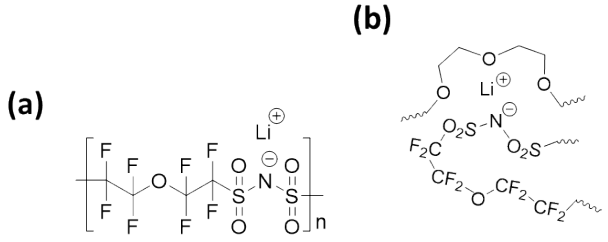

Figure 13. Structure of (a) PFSI ionenes with Li^+ counterions and (b) illustration of the interaction between PFSI ionenes and PEG segments with mobile Li^+ ions by Shi et al.[67]

2.1.4. Nanoparticle synthesis applications

Several works noted that ionenes can be used as a polycationic stabilizer for synthesizing nanoparticles.[68–71] The aggregation of nanoparticles can be detected by changes in color, for instance, orange-brown to gray-blue for silver nanoparticles (AgNPs) and ruby to blue for gold nanoparticles (AuNPs).[69,70] As such, colorimetric techniques using these nanoparticles to sense anions have been suggested. Terenteva et al. stabilized AgNPs using the non-segmented cationic 6,6-ionenes with Br^- counterions to detect the presence of sulfates or pyrophosphate in water.[68,69] The 6,6-ionenes with Br^- counterions also stabilized AuNPs due to the electrostatic repulsion between ionenes and AuNPs and steric stabilization that hindered the aggregation of nanoparticles in order to detect the sulfates in water as shown in **Figure 14.**[71] It was noted that Br^- counterions adsorbed on the surface of AuNPs and recruited ionene adsorption to the surface; the ionene-modified AuNPs were stable in solution for more than 4 months.

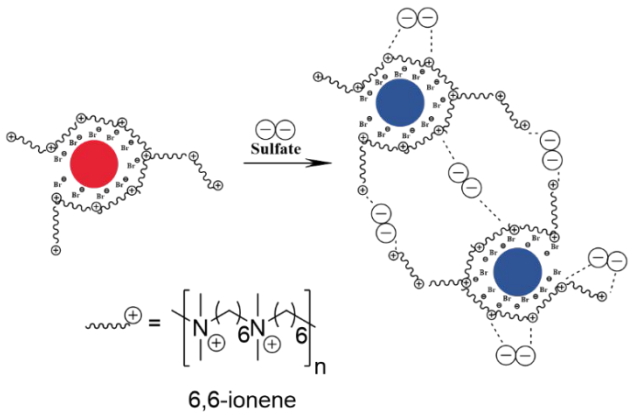

Figure 14. Schematic of a colorimetric technique that uses nanoparticles stabilized by 6,6-ionenes to sense sulfate ions.[71] Reprinted from Ref. 71, Copyright 2015, with permission from Elsevier.

2.1.5. Absorbent materials

Ionenes have been applied as absorbents for the removal of anionic dyes or to separate oil from water. In either case, the adsorptive property is driven by the interaction between the positive charges on the cationic ionene and the negative charges on the dye or oil. A sulfonate dye molecule remains in water longer and demonstrates lower adsorption on common adsorbents when compared to cationic dyes.[72] As an example, silica nanofibers were modified with an aliphatic non-segmented 2,3-ionene (**Figure 15**), which exhibited improved adsorption of a sulfonate-based Acid yellow dye when compared to unmodified nanofibers.[72]

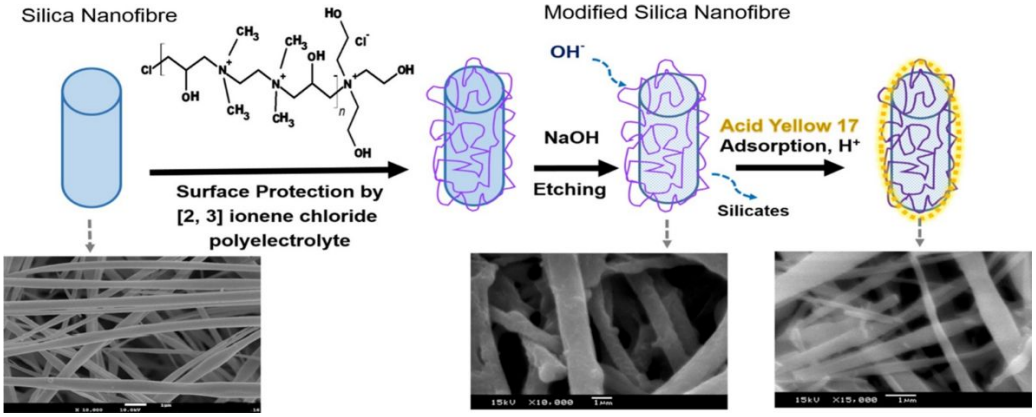

Figure 15. Schematic showing the modification of electrospun silica nanofibers with 2,3-ionenes.[72] Reprinted from Ref. 72, Copyright 2018, with permission from Elsevier.

Dragan et al. introduced DABCO-based polyamide ionenes containing Cl^- counterions for the removal of 3 different azo dyes, Methyl Orange (MO), Ponceau SS (PSS), and Chicago Sky Blue 6B (DB1).[73] The MO, PSS, and DB1 dyes have 1, 2, and 4 sulfonate groups, respectively. Three different DABCO-based polyamide ionenes with different structural isomers of phenylenediamine, *ortho*- (**Figure 16a**), *meta*- (**Figure 16b**) and *para*- (**Figure 16c**), induced adsorption of the dyes onto the ionenes that was dependent on the dye structure and the topology of the ionenes. MO preferably bound onto all of the *meta*-, *ortho*- and *para*-linked isomers of the DABCO-based polyamide ionenes, PSS bound onto the *meta*- and *ortho*-linked isomers of the ionenes, and DB1 bound only onto the *para*-linked isomer of the ionenes.

Pirogov et al. demonstrated that using rigid aromatic ionenes, such as 3,X-ionene, as sorbents for aromatic acids was favorable over aliphatic analogs (e.g., 3,8-ionenes) due to π-π interactions between the sorbent and sorbate.[74] Furthermore, Mansur et al. prepared nanocomposites consisting of 2,y-ionenes (y = 4, 6, 10, and 12) and bentonite to remove oil from oily water.[75] Adding the ionenes improved the removal efficiency by up to ~90% compared to the only bentonite without ionenes. The ionenes intercalated into the bentonite and increased the clay basal space result from the increase of adsorption; however, despite a systematic increase in basal space with an increase in y, the oil removal efficiency was not dependent on y.

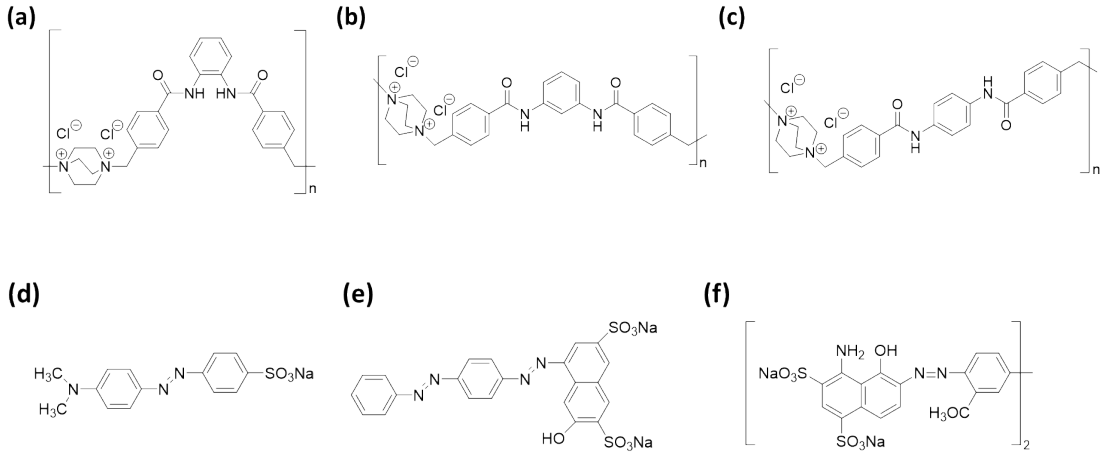

Figure 16. DABCO-based polyamide ionenes having different structural isomers of phenylenediamine (a) *ortho*-, (b) *meta*-, and (c) *para*- position synthesized by Dragan et al.[73] and (d), (e), and (f) represent structures of MO, PSS, and DB1 dyes, respectively.

2.1.6. Other applications

The previously mentioned *meta*-positioned cationic DABCO-based polyamide ionenes (**Figure 16b**) that was used as a dye adsorbent was also used as an n-doping agent in poly(3,4-ethylenedioxythiophene) (PEDOT) for electrochemical devices.[76] The film that was n-doped with ionenes exhibited better thermal stability and was more hydrophilic than the film

n-doped with tetramethylammonium owing to the presence of polar amide groups in the ionene. Later, an imidazolium ionic liquid (1-ethyl-3-methylimidazolium with Tf_2N^- counterions) better stabilized the negative charge of the n-doped PEDOT, showing a higher n-doping concentration than an ammonium cation.[77] This suggests that using imidazolium-based ionenes instead of ammonium-based ionenes could improve the performance of electrochemical devices.

2.2 Hydrogels

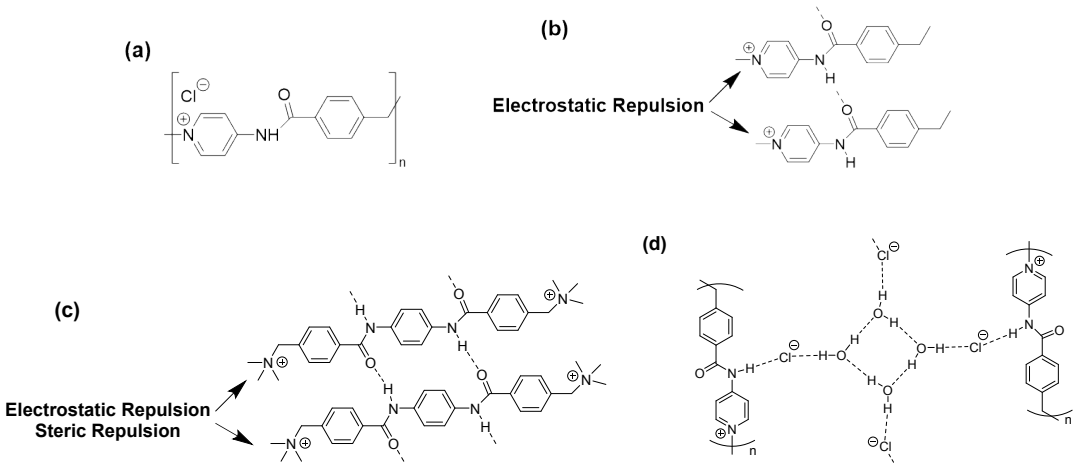

Figure 17. (a) Structure of the pyridinium-based polyamide ionene and illustration of the possible hydrogen bonding (b, c) between amide groups, and (d) mediated by the Cl^- counterions reported by Yoshida et al.[82]

Solvent-swollen gels can be categorized as either hydrogels or organogels depending on the solvents (i.e., water or an organic solvent). Hydrogels are promising candidates for biomaterials due to their favorable swelling behavior that mimic biological tissue and they have also been used in fuel cells and batteries.[78–80] For the physically crosslinked hydrogel using the cationic ionenes, the driving force of the gelation is weak and non-covalent interactions such as hydrogen bonding, van der Waals, π-π stacking, and electrostatic forces between the gelator molecules and a reversible thermal-phase transition between gel and sol sates is their main feature.[81] The Yoshida group created pyridinium-based ionene hydrogels containing a

benzamide group and Cl^- counterions (**Figure 17a)** and hydrogen bonds between the amide groups (**Figure 17b and 17c**), and the amide group the Cl^- counterions and water (**Figure 17d**) caused the gel to form.[82] At higher concentrations (30 g/L) the ionene hydrogel started to collapse at 10% strain, but it recovered rapidly, which is a common property for ionene-based hydrogels. Moreover, the incorporation of single-walled carbon nanotubes (0.1 g/L) decreased the T_{gel} of the hydrogel (20 g/L) from ca. 80 ℃ to ca. 56 ℃. The addition of inorganic salts increased the T_{gel} gradually due to the salt-in behavior.[83] The brittleness of the hydrogel increased with an increasing salt concentration because the hydrogel became more tightly packed and formed a stronger network. The hydrogel began precipitating at a certain salt concentration (i.e., 0.07 mM for NaCl and 0.04 mM for NaBr) owing to the excessive network formation which collapses the network structure, and the presence of salt also reduced the recovery process. The ionenes with Cl^- counterions formed a gel even in acid, pH 1, in contrast to natural gelators. The Yoshida group exchanged the counterions by a simple anion exchange reaction to examine the ionene solubility in various solvents (summarized in **Table 1**).[84] Overall, by simply exchanging anionic counterions on the pyridinium-based polyamide ionenes, they dramatically changed the solubility in organic solvents. Misawa et al. synthesized DABCO-based polyamide ionenes and ammonium-based polyamide ionene hydrogels containing with Cl^- counterions as shown in **Figure 18ai**.[85] The intermolecular hydrogen bonding between amide groups induced a gel network as confirmed by the vial inversion method (**Figure 18aii**). DABCO-based ionenes at 50 g/L took 3 days to produce hydrogels in water with heat, whereas aliphatic ammonium ionenes at 30 g/L took only 5 h due to the flexible ethylene linker. Although the higher concentration of the ionenes caused the gel to be brittle, the gelation time decreased with an increase in the concentration. The length of the alkylene spacer between ionic groups affected the gelation time; a spacer with six methylene units

formed a gel after 3 h at 10 g/L whereas two and three methylene units formed a gel after 5 h and 3-4 d at 30 g/L, respectively. Diaz and coworkers examined DABCO-based polyamide ionenes with Cl^- counterions (**Figure 16)**, but compared *para*-linked phenylenediamine with *ortho*- and *meta*-linked analogs.[86] The computational studies predicted that the *ortho*-linker was the most suitable to form a stable hydrogel due to the complex and dense hydrogen bonding and π-π stacking interaction network, although the *meta*-positioned linker had more abundant interactions (**Figure 18b**). The difference in the molecular structure influenced the gelation kinetics and critical gelation concentration (CGC). The *ortho*-linker had a four and two-fold lower CGC than *meta*- and *para*-linkers, respectively as well as the fastest gelation time at a consistent concentration, but also the gel-to-sol transition occurred by sonication rather than heating. Moreover, *ortho*-linked DABCO-based polyamide ionenes containing Cl^- counterions formed better gels in solutions of varying pH and ionic strength when compared to *meta*- and *para*-linked ionenes due to the synergistic effect of polymer-polymer interactions and polymer-counterion interactions, while *meta*- and *para*-linked ionenes showed only singular trends.[18] Separately, the authors demonstrated that *ortho*-linked hydrogels exhibited self-healing properties and that they could be injected through a 21-gauge needle into various shapes for biomedical applications (**Figure 18c**).[87]

Table 1. Solubility and gelation ability based on the type of counterions (No: insoluble; Yes: soluble; Gel: formed a gel at 1 wt% concentration).[84]

Solvent	Cl^-	BF_4^-	PF_6^-	Tf_2N^-	BPh_4^-	I^-	SCN^-	DCA^-	ClO_4^-	$CF_3SO_3^-$
DMA	No	Yes	Yes	Yes	Yes	Gel	Yes	No	Yes	Yes
DMSO	No	Yes	Yes	Yes	Yes	Yes	Yes	Yes	Yes	Yes
DMF	No	Yes	Yes	Yes	Yes	Gel	Yes	Yes	Yes	Yes

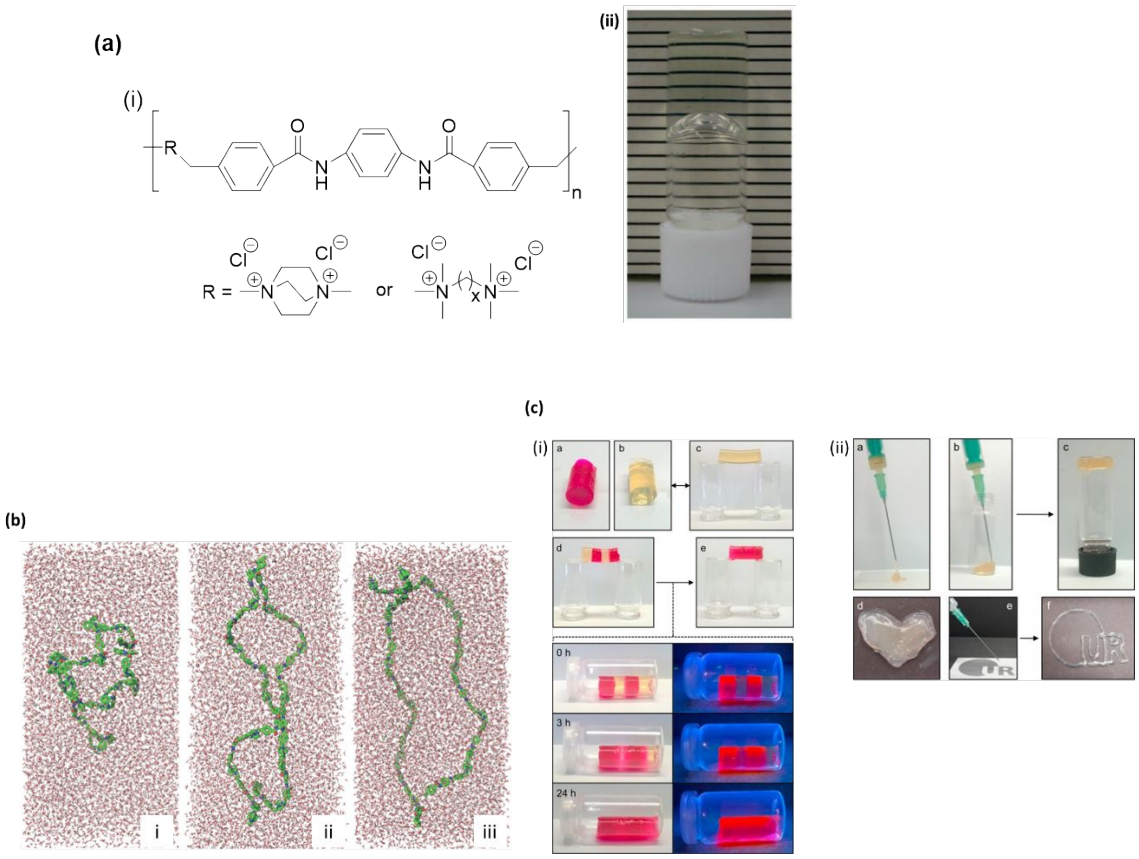

Figure 18. (a) Structure of the DABCO-based polyamide ionenes and aromatic polyamide ammonium ionene (i) and DABCO-based polyamide ionenes with Cl^- counterion hydrogel (ii).[85] Reprinted with permission from Ref. 85. Copyright 2008 American Chemical Society. (b) computer simulated DABCO-based polyamide ionenes with three different structure. (i : *ortho*-, ii : *meta*-, and iii : *para*-).[86] Reproduced from Ref. 86 with permission, copyright 2014 John Wiley and Sons. (c) illustration of the *ortho*-linked DABCO-based polyamide ionene hydrogel. The fusion of dye doped and undoped gel became a gel bridge after 24 h showing dye diffusion through self-healed gel (i), and showed injectability property (injectable hydrogel) (ii).[87] Reprinted from Ref. 87, Copyright 2019, with permission from Elsevier.

3. Segmented ionenes

Unlike non-segmented ionenes, most segmented ionenes show elastomeric behavior due to the presence of soft and hard repeating segment. Typically, segmented ionenes demonstrate superior mechanical performance and elastic behavior, related to the microphase separation, when compared to non-segmented ionenes. Williams and Long reviewed the state of ionenes in 2009 including a description of segmented ionenes and the varying types of soft segments.[1] However, various segmented ionenes have been reported during the past decade

composed of more diverse soft segments that have not been reviewed. Several oligomeric monomers including PTMO, PEG, and PPG have been used to make ionenes with ammonium, imidazolium, DABCO, or pyridinium ionic groups.[88–90] The elastic nature of the ionenes arises from the ionic clustering induced by electrostatic interactions between the backbone ions and counterions, which produce physical crosslinking points.[91] In surveying the literature, we categorized the segmented ionenes into three types: aliphatic ionenes, aromatic ionenes, and heterocyclic ionenes (e.g., pyridinium, imidazolium, or DABCO charged groups) as shown in **Figure 19**. The soft segment is shown as PTMO in each case for direct comparison, also the charged sites for the aliphatic and aromatic ionenes are shown as ammonium. In this way, it will decouple the role of hard and soft segments and give insights to design future segmented ionenes for various applications.

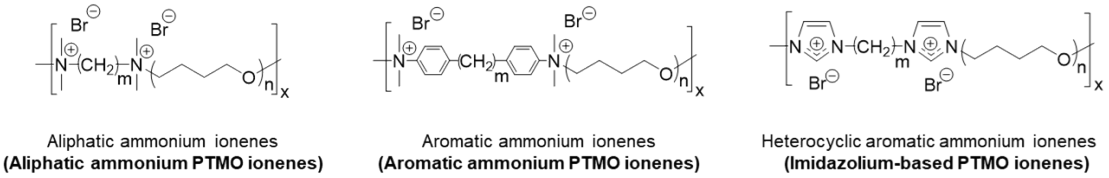

Figure 19. Schematic showing the three types of hard segments in segmented ionenes.

3.1 Elastomer

3.1.1. Aliphatic and aromatic ammonium ionenes

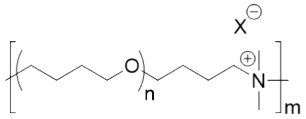

Figure 20. Structure of the aliphatic PTMO mono ammonium ionenes synthesized by Ikeda et al.[92]

Ikeda et al. prepared aliphatic ammonium PTMO ionenes by polymerizing tetrahydrofuran and terminating with N,N-dimethylamino trimethyl silane.[92] Then, the anion

was exchanged by sodium bromide or sodium chloride to introduce Br^- and Cl^- counterions, respectively (**Figure 20**). The ionenes had only one ammonium cation in each repeating unit that caused the ionic segments to weakly aggregate in comparison to diammonium cations in each repeating unit, and thus exhibited a short rubbery plateau region.[93] These results showed how the type of counterion could change the mechanical properties and the morphology of ionenes. Br^- counterions aggregated more tightly and stably relative to Cl- counterions, inhibited room-temperature crystallization in the soft segment, and also promoted strain-induced crystallization, all of which increased the ultimate tensile stress and produced a flatter rubbery plateau region (**Figure 21)**.

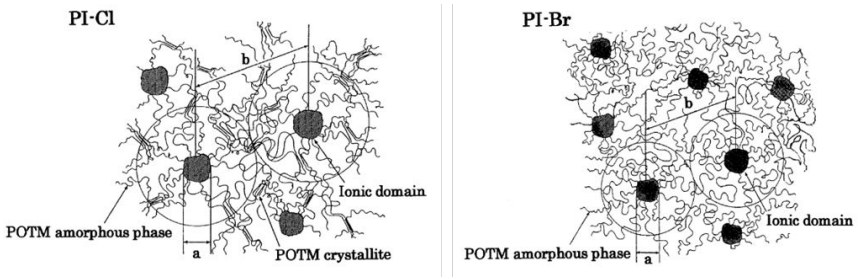

Figure 21. Schematic of the effect of counterions on the morphology of aliphatic ammonium PTMO ionenes at room temperature (PI-Cl: PTMO ionenes containing Cl^- counterions, and PI-Br: PTMO ionenes containing Br^- counterions).[92] Reprinted from Ref. 92, Copyright 2004, with permission from Elsevier.

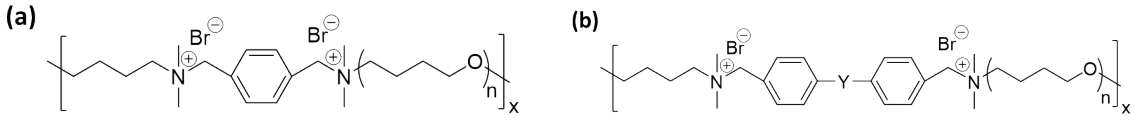

Figure 22. (a) Structure of the aromatic PTMO ammonium ionenes using dimethylamino terminated PTMO and 1,4-dibromo-*p*-xylene reported by Feng et al.[94] (b) structure of aromatic PTMO ammonium ionenes containing a variable spacer group between benzyl groups reported by Feng et al.[11]

Feng et al. prepared an aromatic ammonium PTMO ionene containing Br^- counterions by reacting dimethylamino terminated PTMO with 1,4-dibromo-*p*-xylene (**Figure 22a**); the ionenes displayed no PTMO crystallization at room temperature when the M_n was < 3,400

g/mol.[11,94] Transmission electron microscopy (TEM) revealed cylindrical ionic domains and increasing the PTMO molecular weight from 1,800 g/mol to 6,600 g/mol decreased the volume fraction of the ionic segments leading to randomly distributed ionic domains with weaker phase separation and increased d-spacing. Ikeda et al. also studied segmented pyridinium-based PTMO ionenes in which reducing the PTMO molecular weight caused PTMO chain extension because of stronger Coulombic interaction energies per unit volume (when PTMO M_n < ~5,000 g/mol).[95,96] Moreover, the increase of the PTMO molecular weight from 3,400 g/mol to 10,000 g/mol decreased the tensile strength (from 45 MPa to 30 MPa), strain at break (between ca. 900-1200%), and rubbery plateau modulus due to the induced lower portion of hard segments.[11] Aromatic PTMO ionenes with an aliphatic ether spacer group between dibenzyl halide, Y in **Figure 22b**, showed a lower stress at a given elongation compared to the non-spacer group (No Y) due to three potential reasons: poor phase separation due to weaker ionic association; a higher degree of hard-soft segment mixing, and/or interactions between two benzyl halide due to the flexible ether linkage. Generally, the incorporation of the spacer group decreased the rubbery plateau modulus due to the weaker overall association of the ionenes. Furthermore, regardless of the presence of spacer group, ionenes containing Cl^- counterions showed a higher stress at a given elongation and a lower strain at break than ionenes containing Br^- counterions due to the smaller size and greater electronegativity of Cl^-, which promotes better packing and Coulombic interactions and, thus, provides a stronger ionic association in the aromatic PTMO ionenes.

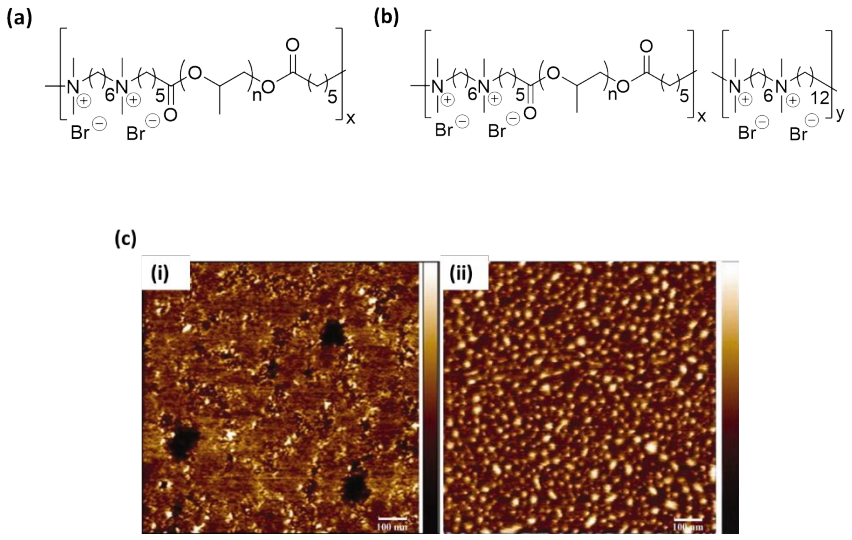

Figure 23. Structure of the aliphatic ammonium PPG ionenes having (a) bromine end-capped PPG with one hard segment, and (b) copolymerized with two hard segments synthesized by Tamami et al.[17]. (c) microphase separation of segmented ionenes having 1k PPG (i) and 4k PPG (ii) revealed by atomic force microscopy.[17] Reproduced from Ref. 17 with permission, copyright 2010 John Wiley and Sons.

Unlike PTMO that crystallizes at ambient temperature, the amorphous PPG does not crystallize even at high molecular weight. Tamami et al. studied the effect of the PPG soft segment molecular weight on the characteristics of aliphatic ammonium ionenes with Br^- counterions (**Figure 23a**).[17] The higher concentration of hard segments reduced the thermal stability, decreasing the onset of degradation temperature from ca. 250 °C to 210 °C. The higher charge density also increased the rubbery plateau modulus, potentially due to higher hard segment content that reduces chain mobility. The authors also prepared copolymers to study the effect of charge density by supplementing the hard segment with a 1,12-dibromododecane comonomer (**Figure 23b**). Decreasing the soft segment molecular weight reduced the viscous flow temperature due to fewer chain entanglements as well as microphase separation (**Figure 23c**), but increased the rubbery plateau modulus and stress during elongation due to the high charge density. Interestingly, when the PPG soft segment molecular weight was kept constant at 1,000 g/mol and the charge density was altered via copolymerization, an increase in the hard

segment content from 12 wt% to 33 wt% caused the rubbery plateau modulus to increase two orders of magnitude. Based on this research, design strategies to modify the charge density of ionenes through soft segment molecular weight and copolymerization are conceived to alter the mechanical properties and microphase separation of segmented ionene elastomers. Hall and coworkers showed that the decrease of PPG content from 70% to 29% in aliphatic ammonium PPG copolymer ionenes increased the microphase separation and local ionic aggregation via molecular dynamics simulations using a coarse-grained model.[97] Moreover, the microphase separation increased with decreasing temperature.

The 7,7,8,8-tetracyano-quinodimethane (TCNQ) salt, which is a strong electron acceptor, has been used for conducting polymers due to its high electrical conductivity.[98] It has been shown that carrier electrons move through the TCNQ moiety and polycations arrange the TCNQ salt.[99] Ionenes with $TCNQ^-$ counterions showed higher electrical conductivity than the ionomers, and the aliphatic ammonium ionenes had a higher resistivity than aromatic ammonium ionenes.[100,101] Incorporating the rigid ring structure (i.e., pyridinium) in the backbone of ionenes reduced the Coulombic repulsion between counterions, and thus increased the electrical conductivity.[99] The authors also studied a series of aromatic compounds, but found that the structural differences among the aromatic compounds in the ionenes backbone did not show any significant difference in the electrical conductivity of the ionenes with $TCNQ^-$ counterions.[100] However, heterocyclic (DABCO) or heterocyclic aromatic (pyridinium) ammonium ionenes showed rigidity and a large distance between the quaternized nitrogen atoms that enabled $TCNQ^-$ counterions to have a high electrical conductivity.[98] Based on their result, it is noteworthy that an even number of methylene groups between DABCO made polymer chain to be straight whereas an odd number of methylene units caused the polymer to be bent; thus, an even number of methylene groups increased the electrical conductivity.

Pyridinium-based ionenes were not affected by the number of methylene groups between bipyridine because the bipyridine ring is bulkier than DABCO ring.

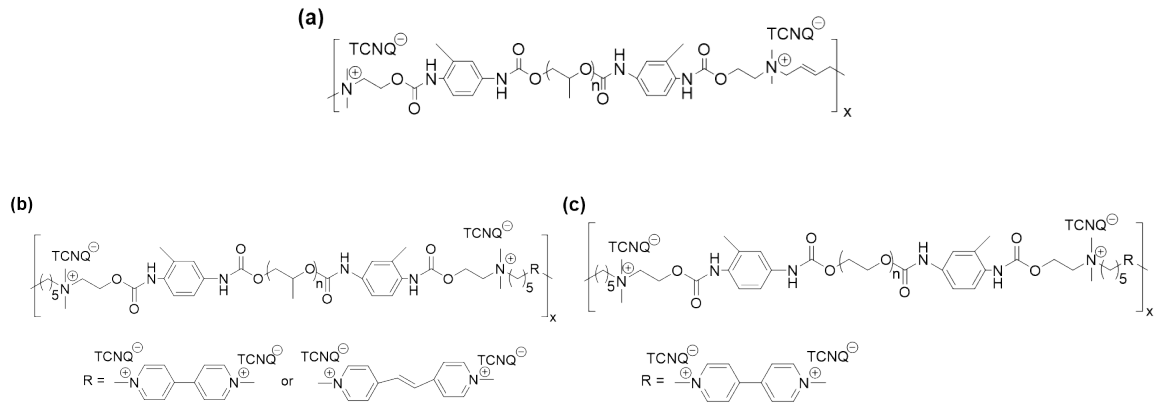

Figure 24. (a) Synthesis of the aromatic ammonium PPG ionenes containing $TCNQ^-$ counterions by Somoano et al.[90] and the structure of the bipyridine incorporated aromatic ammonium (b) PPG ionenes by Watanabe et al.,[88] and (c) PEG ionenes by Takizawa et al.[102] with $TCNQ^-$ counterions.

Although the ionene elastomer is known to have a lower conductivity, it has received great attention due to its useful chemical and physical properties. The Rembaum group reported a conducting elastomer using the aromatic ammonium PPG ionenes with $TCNQ^-$ counterions (**Figure 24a**)[90] wherein the resistivity was inversely proportional to the charge density and directly proportional to the distance between $TCNQ^-$ counterions. An increase in the molecular weight of the PPG soft segment decreased the charge density and the electrical conductivity. Furthermore, Watanabe et al. incorporated the heterocyclic aromatic bipyridine into the aromatic ammonium PPG ionenes with $TCNQ^-$ counterions (**Figure 24b**) and it effectively decreased the resistivity by optimizing the spacing between ionic sites.[88] Takizawa et al. synthesized bipyridine-based aromatic ammonium PEG ionenes with $TCNQ^-$ counterions as shown in **Figure 24c**.[102] The growth of the spherulites due to the incorporation of PEG prevented the formation of a conduction path, but the resistivity significantly decreased at temperatures above the T_m of PEG.

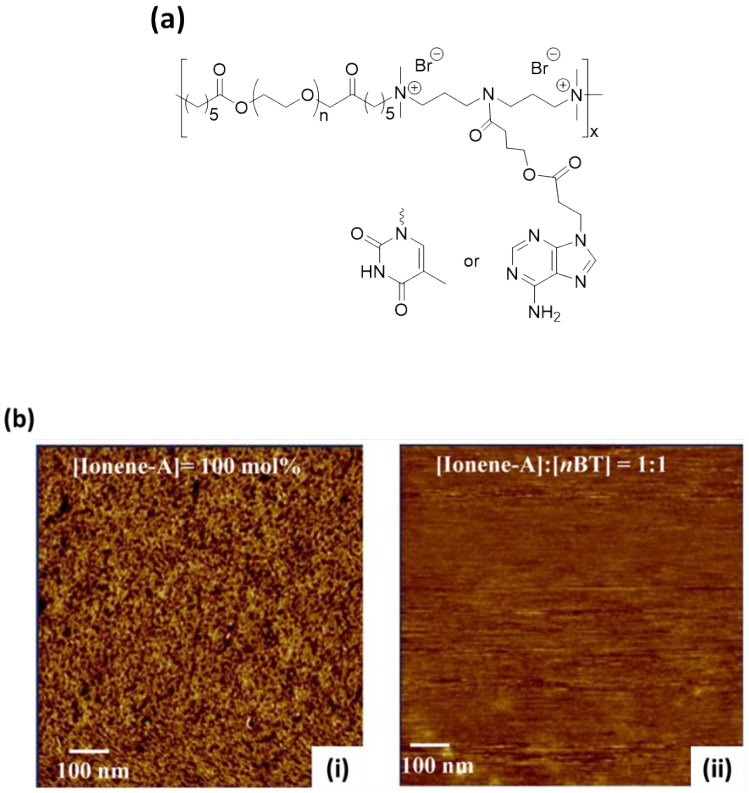

Figure 25. (a) Structure of the aliphatic ammonium PEG ionenes containing nucleobases as a pendent group with Br^- counterions and (b) microphase separation of Ionene-A (i) and Ionene-A with nBT (ii) revealed by atomic force microscopy.[105] Reprinted from Ref. 105, Copyright 2013, with permission from Elsevier.

Burmistr et al. studied the synthesis, thermal properties, and ionic conductivity of aliphatic ammonium PEG ionenes with Cl^- counterions.[103] Increasing the PEG soft segment molecular weight decreased the T_g, transitioned the polymer from amorphous to semi-crystalline, improved microphase separation, and decreased the ionic conductivity due to the reduction of free carriers of charge. The synthesis of aliphatic ammonium PEG ionenes with various pendant functional groups were reported by Dimitrov and Berlinova.[104] The incorporation of zwitterionic and perfluorooctyl functional groups into aliphatic ammonium PEG ionenes decreased the crystallinity and the zwitterionic groups possessed the lowest T_m. Tamami et al. designed and synthesized aliphatic ammonium PEG ionenes containing the adenine and thymine nucleobases as a pendant group with Br^- counterions (**Figure 25a**) to

study the effect of hydrogen bonding between nucleobases and also with guest molecules (n-butyl adenine or n-butyl thymine) on thermal and morphological properties of ionenes.[105] The hydrogen bonds did not affect the T_g of the PEG soft segment and induced shorter Bragg spacing. Moreover, introducing guest molecules disrupted original morphology and decreased the phase contrast revealed by AFM as shown in **Figure 25b**.

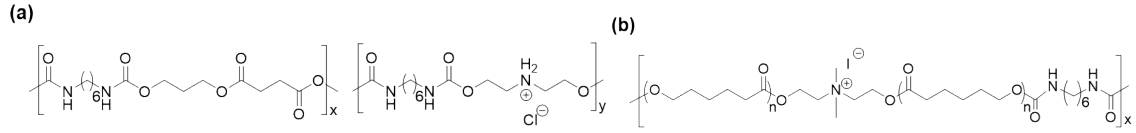

Figure 26. Structure of aliphatic ammonium (a) poly(butylene succinate) (PBS) urethane ionenes containing Cl^- counterions by Wu et al.[106] and (b) poly(caprolactone) (PCL) urethane ionenes containing I^- counterions by Nakayama et al.[107]

Wu et al. reported aliphatic ammonium poly(butylene succinate) (PBS) urethane ionenes containing Cl^- counterions (**Figure 26a**) to study the effect of the urethane ionic hard segment on the properties of the ionenes.[106] The incorporation of the urethane ionic segment decreased the degree of crystallinity of the PBS soft segment without changing the crystal structure, while the crystallization rate was increased because the ionic aggregates promoted urethane alignment. Moreover, the urethane ionic segment increased the hydrophilicity, but did not change the tensile strength and elongation at break which were ca. 40 MPa and ca. 530%, respectively. Also, Nakayama et al. prepared aliphatic poly(caprolactone) (PCL) urethane ammonium ionenes containing I^- counterions (**Figure 26b**).[107] The ionenes were synthesized by mixing hydroxyl-end functionalized PCL, which was polymerized from ε-Caprolactone initiated by N-methyldiethanolamine, and HMDI, and the tertiary amine was quaternized with iodomethane to compare the difference between the urethane polymer and the urethane ammonium ionenes. Modifying the tertiary amine to quaternary ammonium to form ionenes did not change the tensile strength (ca. 30 MPa) but increased the elongation at break (ca. 2,300%) due to the presence of ionic groups. This observation, in contrast to that seen by Wu

et al., could be attributed to the difference in counterion.[106] In addition, the urethane ionenes showed slower biodegradation than uncharged urethane polymers, but the highest molecular weight of PCL (M_n = 13,000 g/mol) did not show slow biodegradation compare to uncharged polymer due to the relatively low charge density.

3.1.2. Heterocyclic ammonium ionenes

3.1.2.1. DABCO-based ionenes (heterocyclic ammonium ionenes)

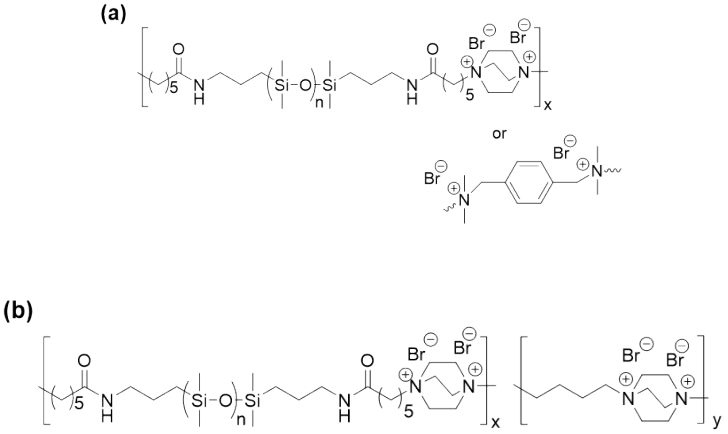

Figure 27. Structure of (a) DABCO-based PDMS ionenes and aromatic ammonium PDMS ionenes, and (b) DABCO-based PDMS ionenes with chain extended DABCO by Das et al.[13]

Das et al. reported DABCO-based copolymer ionenes with Br^- counterions, DABCO/butane hard segments, and poly(dimethylsiloxane) (PDMS) soft segments (**Figure 27**).[13] TGA revealed that the DABCO-based ionenes showed a much higher char yield compared to the xylene-based ionenes due to the bicyclic structure that caused enhanced crosslinking upon exposure to elevated temperature. However, the copolymer ionenes with DABCO/butane-based hard segments showed the lower char yield. The ionenes with chain extended DABCO, which has the highest wt% of hard segments, showed the highest rubbery plateau modulus, which decreased with an increasing molecular weight of PDMS. The xylene-based ionenes exhibited a lower rubbery plateau modulus than DABCO-based ionenes. AFM

showed microphase separation in all ionenes, wherein hard segments formed thread-like domains and dispersed in the PDMS soft segment, and X-ray scattering studies revealed that the hard segments formed cylindrical domains and were oriented in a stretch direction.

3.1.2.2. Imidazolium-based ionenes (heterocyclic aromatic ammonium ionenes)

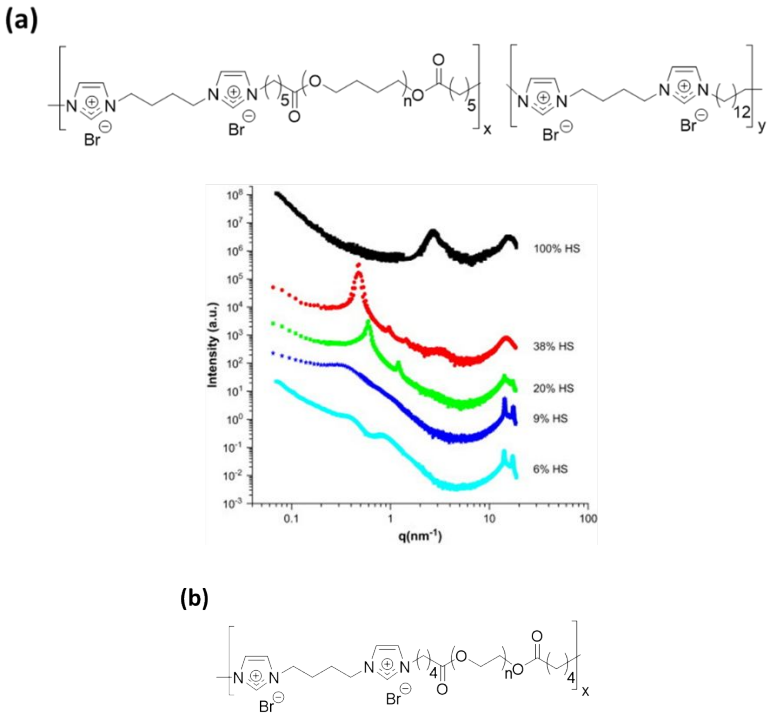

Figure 28. (a) Synthesis of copolymerized imidazolium-based PTMO ionenes copolymers and multi-angle X-ray scattering intensity.[8] Reprinted from Ref. 8, Copyright 2010, with permission from Elsevier. (b) imidazolium-based PEG ionenes by Thankamony et al.[22]

Williams et al. introduced the first copolymer imidazolium-based PTMO ionenes (**Figure 28a**) with bisimidazolium/dodecane hard segments and PTMO soft segments.[8] The increase of hard segments reduced the PTMO crystallinity and showed clearer microphase separation (i.e., at 20 wt% and 38 wt% hard segment multiple scattering peaks at scattering vectors from 0.2 to 2 nm^{-1} were observed). Other literature accounts used imidazolium-based PTMO ionenes to prepare nonwoven fibers using electrospinning.[108] Three different PTMO soft segment molecular weights were used to vary the hard segment content. The tensile

strength increased with an increasing molecular weight of PTMO, which disagrees with other literature that reported a decrease in tensile strength as a function of increasing the soft segment molecular weight.[11,17] The authors observed strain-induced crystallization of PTMO at the higher PTMO molecular weights, which could have accounted for the contradictory trends in tensile performance. Others prepared an imidazolium-based PEG ionenes (**Figure 28b**), which exhibited an outstanding thermal stability (for ionenes) with the onset of degradation occurring at 260 ℃.[22]

3.1.2.3. Pyridinium-based ionenes

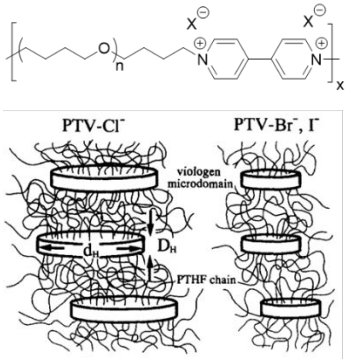

Figure 29. Structure of the pyridinium-based PTMO ionenes and schematic of the effect of counterions on the morphology (PTV-Cl^- : pyridinium-based PTMO ionenes containing Cl^- counterions, and PTV-Br^-, I^- : pyridinium-based PTMO ionenes containing Br^- and I^- counterions, respectively).[91] Reprinted from Ref. 91, Copyright 1994, with permission from Elsevier.

Viologen units have been used as an ionic hard segment in elastomeric segmented ionenes due to their unique structure and properties. The pyridinium-based ionenes display comparable mechanical properties but improved thermal properties compared to aromatic ammonium ionenes.[21] Hashimoto et al. generated pyridinium-based PTMO ionenes, which showed stress-induced crystallization of the PTMO after 300% strain and an increase in the tensile strength at break Cl^- to Br^- and I^- (Cl^-<Br^-<I^-) counterions.[91] This result corroborates findings from previous literature that Br^- counterions have a more significant effect than Cl^-

counterions on the tensile performance of aliphatic PTMO ammonium ionenes.[92] The pyridinium-based ionenes, with all counterions, showed a rubbery plateau region until 150 ℃; however, the ionenes containing Cl^- counterions showed the highest T_m and T_g and the lowest crystallization temperature (T_c) compared to Br^- and I^-. Moreover, the tan δ peak intensity increased in the order of $Cl^-<Br^-<I^-$, corroborating the above results; furthermore, the ionene with the Cl^- counterion had the widest tan δ peak because the crystallites constrained the motion of the amorphous PTMO soft segments. Overall, the pyridinium-based PTMO ionenes with Cl^- counterions showed the highest degree of microphase separation and a schematic of the morphology depicting the lamellar morphology with the disk-like aggregation of the ionic segments based on the SAXS analysis is shown in **Figure 29**.[91] This pyridinium-based PTMO ionenes swelled in room temperature water because the ionic aggregates created physical crosslink points, the polymers absorbed 53.1%, 43.2% and 8.8% water for the Cl^-, Br^- and I^- counterion, respectively.[109] The tensile strength decreased with increasing water content, but the elongation at break did not change substantially. They also showed the photochromic reaction as ionenes containing Cl^- counterions exhibited a color change from colorless to green. A tensile strength relaxation also occurred by light irradiation due to the photoreduction of the viologen group causing changes in the ammonium cation of viologen group into the radical cation and resulting in a decrease in the ionic charge. Meanwhile, ionenes containing Br^- counterions needed poly(N-vinyl-2-pyrrolidone) as an accelerator for the photo-induced reaction, which did not negatively affect the elastic properties of the ionene, to show the color changed and tensile strength relaxation.[110]

Feng et al. determined that the PTMO soft segment in the pyridinium-based PTMO ionenes showed stress-induced crystallization when the PTMO molecular weight was 1,300 g/mol.[21] Also, the tensile strength increased with an increase in the PTMO molecular weight

from 1,300 g/mol to 1,700 g/mol and then decreased with an increase in the PTMO molecular weight from 1,700 g/mol to 2,500 g/mol. These results corroborate the results discussed in the imidazolium-based ionenes section.[108] The tendency toward stress-induced crystallization of PTMO with the increase in the PTMO molecular weight may not be affected by the hard segment or ionic composition.

The pyridinium-based PTMO ionenes using 4,4'-bipyridine hard segments with $CF_3SO_3^-$ counterions showed an unusual 'jump' in the storage modulus at around 50 °C (after melting of PTMO soft segment) due to the conformational, or repacking, changes in the ionic hard segments.[21] In contrast, incorporating methylene groups between hard segments did not cause a modulus 'jump' but showed a weakened ionic association. Furthermore, $CF_3SO_3^-$ counterions in pyridinium ionenes showed weaker ionic aggregation than Cl^-, Br^- and I^- counterions.[91] Ikeda et al. prepared pyridinium-based PTMO ionenes containing Cl^- counterions and 2,2'-bipyridine hard segments.[96] The molecular weight of PTMO was ca. 10,000 g/mol and showed a tensile strength of 34 MPa and an elongation at break of 540%. By comparison, an aromatic ammonium PTMO ionene (also with a 10,000 g/mol PTMO soft segment but with a dibenzyl hard segment and Br^- counterions) showed similar tensile strength and a much higher elongation at break (ca. 900%).[11] This is likely due to the difference in the hard segment moiety or counterions since previous work determined that Br^- counterions improved the tensile performance.[11,91]

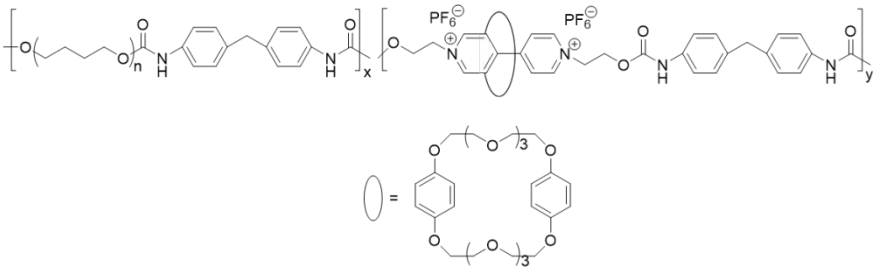

Figure 30. Structure of the copolymerized pyridinium-based PTMO ionenes with rotaxane moiety at the hard segment reported by Loveday et al.[111]

Loveday et al. designed a rotaxane moiety, bis(*p*-phenylene)-30-crown-10, to complex with the hard segment in pyridinium-based PTMO ionenes as shown in **Figure 30**.[111] The presence of the rotaxane moiety enhanced the thermal stability and increased the elastic modulus compared to non-rotaxane analogs. SAXS showed no difference in d-spacing as a function of change in the molecular weight of PTMO. However, Br^- counterions promoted better phase separation and packing (smaller d-spacing and increased peak sharpness) compared to bulky PF_6^- counterions due to the smaller and more electron-dense Br^- counterions.

4. Conclusion

Ionenes have been developed into a variety of diverse and complicated structures, with an ever expanding library of monomers or prepolymers, since their introduction to the literature in 1933. Most reported ionenes are cationic ionenes, which presents an opportunity to develop and investigate the complementary anionic ionenes. Ionenes can also be divided into the categories of segmented and non-segmented ionenes, in a similar fashion to polyurethanes and polyureas. Segmented ionenes have robust thermoplastic elastomer characteristics, but non-segmented ionenes have seen action in a diverse set of applications over the past 10 years. There is still ample room for further investigation to understand the performance of non-segmented ionenes in reported and new applications. Nevertheless, they are a promising

candidate for CO_2 separation membranes and within various biomedical fields due to their high charge density and the interaction between the counterions and the charged polymer backbone. Non-segmented ionenes have been deployed in polymer networks by incorporating crosslinkers and encapsulating ILs for membrane applications. They have recently been studied as hydrogels for biomedical applications. The use of different counterions, different monomeric isomers, and secondary bonds (i.e., hydrogen bonds) results in the production of ionene hydrogels with a range of properties. On the other hand, segmented ionenes have not been fully optimized for other applications. They have numerous advantages including the combination of elasticity, strong mechanical stability, and tunable thermal properties. The majority of reported segmented ionenes include ammonium cations (including heterocyclic DABCO-based ionenes, and heterocyclic aromatic imidazolium and pyridinium-based ionenes), presenting opportunities for different types of ionenes, such as segmented phosphonium-based ionenes. Furthermore, the elastic properties and ionene morphology vary with the structural characteristics, including the soft segment molecular weight, the overall ionene molecular weight, counterion composition, presence of aromatic, heterocyclic or heterocyclic aromatic components, and functional pendant groups. In other words, synthesizing novel segmented ionenes presents a near-infinite research space. The current trends reveal that segmented ionenes have potential for electrochemical and biomedical applications due to their robust and high mechanical, thermal, conductive, and elastic properties that can be designed by various factors. In this work, we highlight the many structural variations in segmented and non-segmented ionenes, and, as often as possible, correlate those structural variations to functional characteristics and desirable properties that were observed.

Author contributions

Jae Sang Lee: Conceptualization, investigation, writing – original draft, and writing – review & editing. Alexis Hocken: Investigation, writing – original draft, and writing – review & editing. Matthew D. Green: Conceptualization, investigation, project administration, supervision, visualization, funding acquisition, writing – original draft, and writing – review & editing.

Conflicts of interest

There are no conflicts to declare.

Acknowledgements

The authors wish to thank the Army Research Office (W911NF-18-1-0412) and NASA (80NSSC18K1508) for financial support.

References

1 S. R. Williams and T. E. Long, *Prog. Polym. Sci.*, 2009, **34**, 762–782.

2 S. R. Williams, T. E. Long, T. C. Ward, S. R. Turner and M. Roman, *Dissertation*.

3 J. E. Bara and K. E. O'Harra, *Macromol. Chem. Phys.*, 2019, **220**, 1900078.

4 C. F. Gibbs, E. R. Littmann and C. S. Marvel, *J. Am. Chem. Soc.*, 1933, **55**, 753–757.

5 A. Rembaum, W. Baumgartner and A. Eisenberg, *J. Polym. Sci. Part B Polym. Lett.*, 1968, **6**, 159–171.

6 W. H. Daly and H. J. Hölle, *J. Polym. Sci. Part B Polym. Lett.*, 1972, **10**, 519–525.

7 Q. Shi, L. Xue, Z. Wei, F. Liu, X. Du and D. D. DesMarteau, *J. Mater. Chem. A*, 2013, **1**, 15016.

8 S. R. Williams, D. Salas-de la Cruz, K. I. Winey and T. E. Long, *Polymer (Guildf).*, 2010, **51**, 1252–1257.

9 S. Das, I. Yilgor, E. Yilgor, B. Inci, O. Tezgel, F. L. Beyer and G. L. Wilkes, *Polymer (Guildf).*, 2007, **48**, 290–301.

10 S. Kohjiya, T. Ohtsuki and S. Yamashita, *Die Makromol. Chemie, Rapid Commun.*, 1981, **2**, 417–420.

11 D. Feng, L. N. Venkateshwaran, G. L. Wilkes, C. M. Leir and J. E. Stark, *J. Appl. Polym. Sci.*, 1989, **38**, 1549–1565.

12 M. Z. Wang, D. S. Li, X. L. Luo and D. Z. Ma, *J. Polym. Sci. Part B Polym. Phys.*, 1999, **37**, 2928–2940.

13 S. Das, J. D. Goff, S. Williams, D. Salas-De La Cruz, J. S. Riffle, T. E. Long, K. I. Winey and G. L. Wilkes, *J. Macromol. Sci. Part A*, 2010, **47**, 215–224.

14 M. Rutkowska, *J. Appl. Polym. Sci.*, 1986, **31**, 1469–1482.

15 A. Rembaum and H. Noguchi, *Macromolecules*, 1972, **5**, 261–269.

16 A. N. Zelikin, N. I. Akritskaya and V. A. Izumrudov, *Macromol. Chem. Phys.*, 2001, **202**, 3018–3026.

17 M. Tamami, S. R. Williams, J. K. Park, R. B. Moore and T. E. Long, *J. Polym. Sci. Part A Polym. Chem.*, 2010, **48**, 4159–4167.

18 J. Bachl, O. Bertran, J. Mayr, C. Alemán and D. Díaz Díaz, *Soft Matter*, 2017, **13**, 3031–3041.

19 K. Suzuki, M. Yamaguchi, S. Hotta, N. Tanabe and S. Yanagida, *J. Photochem. Photobiol. A Chem.*, 2004, **164**, 81–85.

20 S. T. Hemp, M. Zhang, M. H. Allen, S. Cheng, R. B. Moore and T. E. Long, *Macromol. Chem. Phys.*, 2013, **214**, 2099–2107.

21 D. Feng, G. L. Wilkes, B. Lee and J. E. McGrath, *Polymer (Guildf).*, 1992, **33**, 526–535.

22 R. L. Thankamony, H. Chu, S. Lim, T. Yim, Y.-J. Kim and T.-H. Kim, *Macromol. Res.*, 2015, **23**, 38–44.

23 N. Matsumi, K. Sugai, M. Miyake and H. Ohno, *Macromolecules*, 2006, **39**, 6924–6927.

24 M. Druchok, V. Vlachy and K. A. Dill, *J. Chem. Phys.*, 2009, **130**, 134903.

25 P. Rodič, M. Bratuša, M. Lukšič, V. Vlachy and B. Hribar-Lee, *Colloids Surfaces A Physicochem. Eng. Asp.*, 2013, **424**, 18–25.

26 M. Lukšič, B. Hribar-Lee, R. Buchner and V. Vlachy, *Phys. Chem. Chem. Phys.*, 2009, **11**, 10053.

27 M. Lukšič, R. Buchner, B. Hribar-Lee and V. Vlachy, *Macromolecules*, 2009, **42**, 4337–4342.

28 M. Tamami, D. Salas-de la Cruz, K. I. Winey and T. E. Long, *Macromol. Chem. Phys.*, 2012, **213**, 965–972.

29 W. H. Meyer, R. R. Rietz, D. Schaefer and F. Kremer, *Electrochim. Acta*, 1992, **37**, 1491–1494.

30 N. J. Haskins and R. Mitchell, *Analyst*, 1991, **116**, 901–903.

31 P. Charlier, R. Jérome, P. Teyssié and R. E. Proud'Homme, *J. Polym. Sci. Part A Polym. Chem.*, 1993, 31, 129–134.

32 T. Tsutsui, R. Tanaka and T. Tanaka, *J. Polym. Sci. Polym. Phys. Ed.*, 1976, **14**, 2259–2271.

33 I. Kammakakam, K. E. O'Harra, G. P. Dennis, E. M. Jackson and J. E. Bara, *Polym. Int.*, 2019, **68**, 1123–1129.

34 M. S. Mittenthal, B. S. Flowers, J. E. Bara, J. W. Whitley, S. K. Spear, J. D. Roveda, D. A. Wallace, M. S. Shannon, R. Holler, R. Martens and D. T. Daly, *Ind. Eng. Chem. Res.*, 2017, **56**, 5055–5069.

35 I. Kammakakam, A. H. N. Rao, H. W. Yoon, S. Nam, H. B. Park and T.-H. Kim, *Macromol. Res.*, 2014, **22**, 907–916.

36 P. Li and M. R. Coleman, *Eur. Polym. J.*, 2013, **49**, 482–491.

37 P. Li, Q. Zhao, J. L. Anderson, S. Varanasi and M. R. Coleman, *J. Polym. Sci. Part A Polym. Chem.*, 2010, **48**, 4036–4046.

38 K. O'Harra, I. Kammakakam, E. Devriese, D. Noll, J. Bara and E. Jackson, *Membranes (Basel).*, 2019, **9**, 79.

39 S. T. Hemp, M. Zhang, M. Tamami and T. E. Long, *Polym. Chem.*, 2013, **4**, 3582–3590.

40 C. J. Bradaric, A. Downard, C. Kennedy, A. J. Robertson and Y. Zhou, *Green Chem.*, 2003, **5**, 143–152.

41 X. Yang and R. C. Smith, *J. Polym. Sci. Part A Polym. Chem.*, 2019, **57**, 598–604.

42 S. R. Williams, Z. Barta, S. M. Ramirez and T. E. Long, *Macromol. Chem. Phys.*, 2009, **210**, 555–564.

43 Y. M. Jeon and M. S. Gong, *Polym.*, 2009, **33**, 19–25.

44 M.-S. Gong, *Sensors Actuators B Chem.*, 2010, **148**, 559–568.

45 A. N. Zelikin, A. A. Litmanovich, V. V. Paraschuk, A. V. Sybatchin and V. A. Izumrudov, *Macromolecules*, 2003, **36**, 2066–2071.

46 T. Narita, R. Ohtakeyama, M. Nishino, J. P. Gong and Y. Osada, *Colloid Polym. Sci.*, 2000, **278**, 884–887.

47 A. N. Zelikin, D. Putnam, P. Shastri, R. Langer and V. A. Izumrudov, *Bioconjug. Chem.*, 2002, **13**, 548–553.

48 V. A. Izumrudov and M. V. Zhiryakova, *Macromol. Chem. Phys.*, 1999, **200**, 2533–2540.

49 V. A. Izumrudov, M. V Zhiryakova and S. E. Kudaibergenov, *Biopolymers*, 1999, **52**, 94–108.

50 A. N. Zelikin and V. A. Izumrudov, *Macromol. Biosci.*, 2002, **2**, 78–81.

51 P.-O. Wahlund, V. A. Izumrudov, P.-E. Gustavsson, P.-O. Larsson and I. Y. Galaev, *Macromol. Biosci.*, 2003, **3**, 404–411.

52 H. El-Hamshary, M. H. El-Newehy, M. Moydeen Abdulhameed, A. El-Faham and A. S. Elsherbiny, *Mater. Chem. Phys.*, 2019, **225**, 122–132.

53 E. Tomlinson, M. R. W. Brown and S. S. Davis, *J. Med. Chem.*, 1977, **20**, 1277–1282.

54 X. Liu, H. Zhang, Z. Tian, A. Sen and H. R. Allcock, *Polym. Chem.*, 2012, **3**, 2082.

55 B.-P. Ding, F. Wu, S.-C. Chen, Y.-Z. Wang and J.-B. Zeng, *RSC Adv.*, 2015, **5**, 12423–12433.

56 I. Cakmak, Z. Ulukanli, M. Tuzcu, S. Karabuga and K. Genctav, *Eur. Polym. J.*, 2004, **40**, 2373–2379.

57 S. Venkataraman, J. P. K. Tan, S. T. Chong, C. Y. H. Chu, E. A. Wilianto, C. X. Cheng and Y. Y. Yang, *Biomacromolecules*, 2019, **20**, 2737–2742.

58 Z. Geng and M. G. Finn, *J. Am. Chem. Soc.*, 2017, **139**, 15401–15406.

59 A. Strassburg, J. Petranowitsch, F. Paetzold, C. Krumm, E. Peter, M. Meuris, M. Köller and J. C. Tiller, *ACS Appl. Mater. Interfaces*, 2017, **9**, 36573–36582.

60 M. M. Lakouraj, M. Soleimani and V. Hasantabar, *World Appl. Sci. J.*, 2013, **21**, 250–259.

61 S. Liu, R. J. Ono, H. Wu, J. Yng, Z. Chang, K. Xu, M. Zhang, G. Zhong, J. P. K. Tan, M. Ng, C. Yang, J. Chan, Z. Ji, C. Bao, K. Kumar, S. Gao, A. Lee, M. Fevre, H. Dong, J. Y. Ying, L. Li, W. Fan, J. L. Hedrick and Y. Yan, *Biomaterials*, 2017, **127**, 36–48.

62 M. Berginc, U. Opara Krašovec, M. Jankovec and M. Topič, *Sol. Energy Mater. Sol. Cells*, 2007, **91**, 821–828.

63 A. Abate, A. Petrozza, V. Roiati, S. Guarnera, H. Snaith, F. Matteucci, G. Lanzani, P. Metrangolo and G. Resnati, *Org. Electron.*, 2012, **13**, 2474–2478.

64 Z. Fei, D. Kuang, D. Zhao, C. Klein, W. H. Ang, S. M. Zakeeruddin, M. Grätzel and P. J. Dyson, *Inorg. Chem.*, 2006, **45**, 10407–10409.

65 F. Li, F. Cheng, J. Shi, F. Cai, M. Liang and J. Chen, *J. Power Sources*, 2007, **165**, 911–915.

66 H. M. Ng, S. Ramesh and K. Ramesh, *Electrochim. Acta*, 2015, **175**, 169–175.

67 Q. Shi, L. Xue, D. Qin, B. Du, J. Wang and L. Chen, *J. Mater. Chem. A*, 2014, **2**, 15952–15957.

68 E. A. Terenteva, V. V. Arkhipova, V. V. Apyari, P. A. Volkov and S. G. Dmitrienko, *Sensors Actuators B Chem.*, 2017, **241**, 390–397.

69 E. A. Terenteva, V. V. Apyari, S. G. Dmitrienko and Y. A. Zolotov, *Moscow*

Univ. Chem. Bull., 2015, **70**, 157–161.

70 V. V. Apyari, A. N. Ioutsi, V. V. Arkhipova, S. G. Dmitrienko and E. N. Shapovalova, *Adv. Nat. Sci. Nanosci. Nanotechnol.*, 2015, **6**, 025002.

71 V. V. Arkhipova, V. V. Apyari and S. G. Dmitrienko, *Spectrochim. Acta Part A Mol. Biomol. Spectrosc.*, 2015, **139**, 335–341.

72 M. D. Teli and G. T. Nadathur, *J. Environ. Chem. Eng.*, 2018, **6**, 7257–7272.

73 E. S. Dragan, J. Mayr, M. Häring, A. I. Cocarta and D. D. Díaz, *ACS Appl. Mater. Interfaces*, 2016, **8**, 30908–30919.

74 A. V. Pirogov, O. V. Krokhin, M. M. Platonov, Y. I. Deryugina and O. A. Shpigun, *J. Chromatogr. A*, 2000, **884**, 31–39.

75 C. R. E. Mansur, R. S. Oliveira, V. Akeda, Y. G. C. Queirós, L. S. Spinelli and E. F. Lucas, *J. Appl. Polym. Sci.*, 2012, **123**, 218–226.

76 M. G. Saborío, O. Bertran, S. Lanzalaco, M. Häring, D. Díaz Díaz, F. Estrany and C. Alemán, *Phys. Chem. Chem. Phys.*, 2018, **20**, 9855–9864.

77 A. P. Sandoval, J. M. Feliu, R. M. Torresi and M. F. Suárez-Herrera, *RSC Adv.*, 2014, **4**, 3383–3391.

78 S. K. Kundu, T. Matsunaga, M. Yoshida and M. Shibayama, *J. Phys. Chem. B*, 2008, **112**, 11537–11541.

79 J. Le Bideau, J.-B. Ducros, P. Soudan and D. Guyomard, *Adv. Funct. Mater.*, 2011, **21**, 4073–4078.

80 B. Chen, J. J. Lu, C. H. Yang, J. H. Yang, J. Zhou, Y. M. Chen and Z. Suo, *ACS Appl. Mater. Interfaces*, 2014, **6**, 7840–7845.

81 M. Yoshida, *Chem. Rec.*, 2010, **10**, 230–242.

82 M. Yoshida, N. Koumura, Y. Misawa, N. Tamaoki, H. Matsumoto, H. Kawanami, S. Kazaoui and N. Minami, *J. Am. Chem. Soc.*, 2007, **129**, 11039–11041.

83 S. K. Kundu, M. Yoshida and M. Shibayama, *J. Phys. Chem. B*, 2010, **114**, 1541–1547.

84 N. Koumura, H. Matsumoto, H. Kawanami, N. Tamaoki and M. Yoshida, *Polym. J.*, 2010, **42**, 759–765.

85 Y. Misawa, N. Koumura, H. Matsumoto, N. Tamaoki and M. Yoshida, *Macromolecules*, 2008, **41**, 8841–8846.

86 J. Bachl, D. Zanuy, D. E. López-Pérez, G. Revilla-López, C. Cativiela, C. Alemán and D. D. Díaz, *Adv. Funct. Mater.*, 2014, **24**, 4893–4904.

87 M. Häring, S. Grijalvo, D. Haldar, C. Saldías and D. D. Díaz, *Eur. Polym. J.*, 2019, **115**, 221–224.

88 M. Watanabe, N. Toneaki and I. Shinohara, *Polym. J.*, 1982, **14**, 189–195.

89 B. Grassl and J. C. Galin, *Macromolecules*, 1995, **28**, 7035–7045.

90 R. Somoano, S. P. S. Yen and A. Rembaum, *J. Polym. Sci. Part B Polym. Lett.*, 1970, **8**, 467–479.

91 T. Hashimoto, S. Sakurai, M. Morimoto, S. Nomura, S. Kohjiya and T. Kodaira, *Polymer (Guildf).*, 1994, **35**, 2672–2678.

92 Y. Ikeda, J. Yamato, T. Murakami and K. Kajiwara, *Polymer (Guildf).*, 2004, **45**, 8367–8375.

93 Y. Ikeda, T. Murakami, H. Urakawa, S. Kohjiya, R. Grottenmuller and M. Schmidt, *Polymer (Guildf).*, 2002, **43**, 3483–3488.

94 D. Feng, G. L. Wilkes, C. M. Leir and J. E. Stark, *J. Macromol. Sci. Part A - Chem.*, 1989, **26**, 1151–1181.

95 D. Feng and G. L. Wilkes, *Macromolecules*, 1991, **24**, 6788–6790.

96 Y. Ikeda, T. Murakami, Y. Yuguchi and K. Kajiwara, *Macromolecules*, 1998, **31**, 1246–1253.

97 P. Vijayaraghavan, J. R. Brown and L. M. Hall, *Macromol. Chem. Phys.*, 2016, **217**, 930–939.

98 T. Kamiya, K. Goto and I. Shinohara, *J. Polym. Sci. Polym. Chem. Ed.*, 1979, **17**, 561–569.

99 T. Kamiya, S. Tsuji, K. Ogatsu and I. Shinohara, *Polym. J.*, 1979, **11**, 219–226.

100 G. C. Hochberg, *Polym. Int.*, 1995, **38**, 119–124.

101 W. Ciesielski, J. Pęcherz and M. Kryszewski, *Acta Polym.*, 1982, **33**, 318–321.

102 Y. Takizawa, H. Aiga, M. Watanabe and I. Shinohara, *J. Polym. Sci. Polym. Chem. Ed.*, 1983, **21**, 3145–3153.

103 M. V. Burmistr, K. M. Sukhyy, V. V. Shilov, P. Pissis, G. Polizos, A. Spanoudaki and Y. P. Gomza, *Solid State Ionics*, 2005, **176**, 1787–1792.

104 I. V. Dimitrov and I. V. Berlinova, *Macromol. Rapid Commun.*, 2003, **24**, 551–555.

105 M. Tamami, S. T. Hemp, K. Zhang, M. Zhang, R. B. Moore and T. E. Long, *Polymer (Guildf).*, 2013, **54**, 1588–1595.

106 F. Wu, C.-L. Huang, J.-B. Zeng, S.-L. Li and Y.-Z. Wang, *Polymer (Guildf).*, 2014, **55**, 4358–4368.

107 Y. NAKAYAMA, N. MATSUBARA, R. TANAKA, Z. CAI, T. SHIONO, H. SHIRAHAMA and C. TSUTSUMI, *J. Japan Inst. Energy*, 2014, **93**, 916–920.

108 C. Schreiner, A. T. Bridge, M. T. Hunley, T. E. Long and M. D. Green, *Polymer (Guildf).*, 2017, **114**, 257–265.

109 S. Kohjiya, T. Hashimoto and S. Yamashita, *J. Appl. Polym. Sci.*, 1992, **44**, 555–559.

110 T. Hashimoto, S. Kohjiya, S. Yamashita and M. Irie, *J. Polym. Sci. Part A Polym. Chem.*, 1991, **29**, 651–655.

111 D. Loveday, G. L. Wilkes, M. C. Bheda, Y. X. Shen and H. W. Gibson, *J. Macromol. Sci. Part A*, 1995, **32**, 1–27.